

# Axial-vector form factors of the baryon decuplet with flavor SU(3) symmetry breaking

Yu-Son Jun,<sup>1,\*</sup> Jung-Min Suh,<sup>1,†</sup> and Hyun-Chul Kim<sup>1,2,‡</sup>

<sup>1</sup>*Department of Physics, Inha University, Incheon 22212, Republic of Korea*

<sup>2</sup>*School of Physics, Korea Institute for Advanced Study (KIAS), Seoul 02455, Republic of Korea*

(Dated: June 12, 2022)

The axial-vector form factors and axial-vector constants of the baryon decuplet are investigated within a pion mean-field approach, which is also known as the chiral quark-soliton model. Given an axial-vector current with a specified flavor, there are four different form factors of a decuplet baryon. When we consider the singlet, triplet, and octet axial-vector currents, we have twelve different form factors for each member of the baryon decuplet. We compute all these axial-vector form factors of the baryon decuplet, taking into account the rotational  $1/N_c$  corrections and effects of flavor SU(3) symmetry breaking. We find that, for a given flavor, two of the form factors for a decuplet baryon are only independent within the present approach. We first examine properties of the axial-vector form factors of the  $\Delta^+$  isobar and  $\Omega^-$  hyperon. We also compare the results of the triplet axial-vector form factors of  $\Delta^+$  with those from lattice QCD and those of the present work for the axial-vector constants of the baryon decuplet with the lattice data. All the results for other members of the baryon decuplet are then presented. The results of the axial charges are compared with those of other works. The axial masses and axial radii are also discussed.

Keywords: Baryon decuplet, axial-vector form factors, pion mean fields, the chiral quark-soliton model

arXiv:2005.06824v1 [hep-ph] 14 May 2020

---

\* E-mail: ysjun@inha.edu

† E-mail: suhjungmin@inha.edu

‡ E-mail: hchkim@inha.ac.kr

## I. INTRODUCTION

The axial-vector current probes multi-faceted structures of a baryon. For example, the flavor singlet axial-vector constant of the proton provides its spin content, which is identified as the first moment of the longitudinally polarized spin structure function of the proton [1]. On the other hand, it is well known that the triplet axial-vector constant or the axial charge contains essential information on the neutron beta decay. Moreover, this axial charge can be related to the  $\pi NN$  coupling constant by the Goldberger-Treiman relation [2]. It indicates that the axial-vector constants play a very important role in understanding the structure of a baryon both in strong and weak interactions. While the axial-vector structures of the baryon octet are relatively well known by their semileptonic decays, those of the baryon decuplet are still much less understood, since almost all members of the decuplet decay strongly except for the  $\Omega^-$  baryon. Thus, it is very difficult to get access to the internal structure of them. However, since the lattice data on the axial-vector form factors and the axial-vector constants of the baryon decuplet are now available [3, 4], we anticipate that lattice QCD will provide more information on the axial-vector structure of the baryon decuplet in the near future. While it is rather difficult to measure the axial-vector properties of the baryon decuplet experimentally, there have been various theoretical works. For instance, the axial charge of the  $\Delta$  isobar was studied in chiral perturbation theory [5, 6]. In Refs. [7, 8], the axial charges of the  $\Delta$ ,  $\Sigma^*$ , and  $\Xi^*$  were computed within the Goldstone-boson-exchange relativistic constituent quark model (RCQM). Recently, the axial-vector form factors and the axial-vector constants of the baryon decuplet were derived from lattice QCD [3, 4]. The axial charge of  $\Delta^+$  was also studied in the light-cone sum rules (LCSR) [9]. Very recently, the axial charges of the baryon decuplet except for the  $\Omega^-$  baryon were also calculated in a perturbative chiral quark model (PCQM) [10].

In the present work, we want to investigate the axial-vector form factors of the baryon decuplet within the framework of the chiral quark-soliton model ( $\chi$ QSM) [11–13]. The model is based on the pion mean-field approach that was proposed ingeniously by Witten [14, 15]. In the limit of the large number of colors ( $N_c \rightarrow \infty$ ), a baryon can be viewed as a bound state of the  $N_c$  valence quarks by a pion mean field. The presence of the  $N_c$  valence quarks brings about the vacuum polarization that creates a pion mean field. Then the pion mean field influences the valence quarks self-consistently. As a result, they are bound by the pion mean field, so that a baryon emerges as a bound state of the  $N_c$  valence quarks in the form of a chiral soliton. This  $\chi$ QSM has been successfully applied to describe various properties of the lowest-lying baryons including both the light and singly heavy baryons. For example, the model explains very well the electromagnetic form factors of the baryon octet and decuplet [16–18], the axial-vector form factors of the nucleon [19], the scalar form factor [20], tensor charges and tensor form factors [21–24], the gravitational form factors [25], and so on. Very recently, the model was extended to the description of singly heavy baryons. For example, the electromagnetic form factors of the singly heavy baryons both with spin 1/2 and 3/2 were investigated [26, 27]. Thus, we want to examine the axial-vector form factors of the baryon decuplet within the same framework, focusing on the comparison of the present results with those from the lattice QCD [3, 4].

The present paper is organized as follows: In Section II, we recapitulate the axial-vector form factors of the baryon decuplet. In Section III, we show succinctly how to compute them within the framework of the  $\chi$ QSM. In Section IV, we first present the results of the axial-vector form factors of the  $\Delta^+$  isobar and  $\Omega^-$  hyperon, scrutinizing the effects of flavor SU(3) symmetry breaking. In order to compare the present results with those from the lattice data, we first derive the form factors with the pion mass varied from the physical value to unphysical ones. The results are then compared with those from the lattice QCD with the corresponding values of the pion mass employed. We show the results of the axial-vector form factors of all other members of the baryon decuplet, emphasizing the effects of flavor SU(3) symmetry breaking. Finally, we show the results for the axial charges in comparison with those from other approaches. The results of the axial masses and axial radii are also presented. In the last Section we summarize the present work and give outlook for future works.

## II. AXIAL-VECTOR FORM FACTORS OF THE BARYON DECUPLET

The axial-vector current is defined as

$$A_\mu^a(x) = \bar{\psi}(x)\gamma_\mu\gamma_5\frac{\lambda^a}{2}\psi(x), \quad (1)$$

where  $\psi(x)$  denotes the quark field  $\psi = (u, d, s)$  in flavor space. The  $\lambda^a$  stand for the well-known the flavor SU(3) Gell-Mann matrices. The superscript  $a$  represents one of  $a = 0, 3, 8$  that correspond to the singlet, triplet, and octet currents, respectively. By using the Lorentz structure and the consideration of spin, parity, and charge conjugation, we can parametrize the matrix element of the axial-vector current between the baryon decuplet with spin 3/2 in terms

of four different real form factors [3, 28]:

$$\begin{aligned} \langle B(p', J'_3) | A_\mu^a(0) | B(p, J_3) \rangle = & -\bar{u}^\alpha(p', J'_3) \left[ \gamma_\mu \left\{ g_1^{(a)B}(q^2) \eta_{\alpha\beta} + h_1^{(a)B}(q^2) \frac{q_\alpha q_\beta}{4M_B^2} \right\} \right. \\ & \left. + \frac{q_\mu}{2M_B} \left\{ g_3^{(a)B}(q^2) \eta_{\alpha\beta} + h_3^{(a)B}(q^2) \frac{q_\alpha q_\beta}{4M_B^2} \right\} \right] \gamma^5 u^\beta(p, J_3), \end{aligned} \quad (2)$$

where  $M_B$  is the mass of the baryon involved.  $\eta_{\alpha\beta}$  represents the metric tensor of Minkowski space, expressed as  $\eta_{\alpha\beta} = \text{diag}(1, -1, -1, -1)$ .  $q_\alpha$  designates the momentum transfer  $q_\alpha = p'_\alpha - p_\alpha$  and its square is given as  $q^2 = -Q^2$  with  $Q^2 > 0$ .  $J_3$  ( $J'_3$ ) is the eigenvalue of the third component of the spin operator  $\mathbf{J}$  ( $\mathbf{J}'$ ), which is projected along the direction of the momentum  $\mathbf{p}$  ( $\mathbf{p}'$ ).  $u^\alpha(p, J_3)$  is the Rarita-Schwinger spinor that describes a decuplet baryon with spin 3/2 [29], carrying the momentum  $p$  and  $J_3$ , which can be described by the combination of the polarization vector and the Dirac spinor,  $u^\alpha(p, J_3) = \sum_{i,s} C_{1i \frac{1}{2}s}^{\frac{3}{2}J_3} \epsilon_i^\alpha(p) u_s(p)$ . It satisfies the Dirac equation and the auxiliary equations  $p_\alpha u^\alpha(p, J_3) = 0$  and  $\gamma_\alpha u^\alpha(p, J_3) = 0$ .

In the Breit frame, the form factors defined in Eq (2) are expressed in terms of the the spatial parts of the axial-vector current projected by the spherical basis vectors  $\mathbf{e}_n$  [30, 31]

$$\begin{aligned} g_1^{(a)B}(Q^2) &= -\sqrt{\frac{3}{2}} \frac{M_B}{E_B} \langle B(p', 3/2) | \mathbf{e}_1 \cdot \mathbf{A}^a(0) | B(p, 1/2) \rangle, \\ h_1^{(a)B}(Q^2) &= -\sqrt{\frac{3}{2}} \frac{4M_B^5}{E_B^3 Q^2} \left[ \frac{2M_B^2 + Q^2}{2M_B^2} \langle B(p', 3/2) | \mathbf{e}_1 \cdot \mathbf{A}^a(0) | B(p, 1/2) \rangle \right. \\ &\quad \left. - \frac{\sqrt{3}}{2} \langle B(p', 1/2) | \mathbf{e}_1 \cdot \mathbf{A}^a(0) | B(p, -1/2) \rangle \right], \\ g_3^{(a)B}(Q^2) &= -\frac{4M_B^2}{Q^2} \left[ \langle B(p', 3/2) | \mathbf{e}_0 \cdot \mathbf{A}^a(0) | B(p, 3/2) \rangle - \sqrt{\frac{3}{2}} \frac{M_B}{E_B} \langle B(p', 3/2) | \mathbf{e}_1 \cdot \mathbf{A}^a(0) | B(p, 1/2) \rangle \right], \\ h_3^{(a)B}(Q^2) &= \frac{8M_B^6}{E_B^2 Q^4} \left[ 3 \langle B(p', 1/2) | \mathbf{e}_0 \cdot \mathbf{A}^a(0) | B(p, 1/2) \rangle - \frac{\sqrt{3}(2M_B^2 + Q^2)}{\sqrt{2}E_B M_B} \langle B(p', 3/2) | \mathbf{e}_1 \cdot \mathbf{A}^a(0) | B(p, 1/2) \rangle \right. \\ &\quad \left. + \frac{3M_B}{\sqrt{2}E_B} \langle B(p', 1/2) | \mathbf{e}_1 \cdot \mathbf{A}^a(0) | B(p, -1/2) \rangle - \frac{M_B^2 + Q^2}{M_B^2} \langle B(p', 3/2) | \mathbf{e}_0 \cdot \mathbf{A}^a(0) | B(p, 3/2) \rangle \right], \end{aligned} \quad (3)$$

where  $E_B$  denotes the energy of the corresponding baryon, i.e.  $E_B = \sqrt{M_B^2 + Q^2/4}$ , and  $\mathbf{e}_n$  are expressed explicitly in terms of the Cartesian basis vectors  $\mathbf{e}_0 = \hat{z}$ ,  $\mathbf{e}_1 = -(\hat{x} + i\hat{y})/\sqrt{2}$ ,  $\mathbf{e}_{-1} = (\hat{x} - i\hat{y})/\sqrt{2}$ . We want to mention that the form factors  $h_{1,3}^{(a)B}(Q^2)$  are in fact the same as  $g_{1,3}^{(a)B}(Q^2)$  apart from the kinematical factors.

### III. AXIAL-VECTOR FORM FACTORS IN THE CHIRAL QUARK-SOLITON MODEL

The  $\chi$ QSM is constructed by the effective chiral action as a functional of the pseudo-Nambu-Goldstone (pNG) field  $\pi^a$  given as

$$S_{\text{eff}}[\pi^a] = -N_c \text{Tr} \ln D, \quad (4)$$

where  $\text{Tr}$  represents the functional trace running over four dimensional Euclidean space-time, spin, flavor and color spaces. The  $N_c$  is the number of colors.  $D$  designates the one-body Dirac operator defined by

$$D := i\not{D} + iMU^{\gamma_5} + i\hat{m}, \quad (5)$$

where  $M$  stands for the dynamical quark mass and  $U^{\gamma_5}(x)$  denotes the flavor SU(3) chiral field defined by

$$U^{\gamma_5}(x) := \frac{1 + \gamma_5}{2} U(x) + \frac{1 - \gamma_5}{2} U^\dagger(x) \quad (6)$$

where  $U(x) = \exp(i\lambda^a \pi^a(x)/f_\pi)$  with the pion decay constant  $f_\pi$ .  $\hat{m}$  in Eq. (5) represents the current quark mass matrix given as  $\hat{m} = \text{diag}(m_u, m_d, m_s)$  in flavor space. We assume the isospin symmetry in this work, so that the

current quark mass of the up and down quarks are set equal to each other, i.e.  $m_u = m_d$  with their average mass  $\bar{m} = (m_u + m_d)/2$ . Then, the current quark mass matrix is written as  $\hat{m} = \text{diag}(\bar{m}, \bar{m}, m_s) = \bar{m} + \delta m$ .  $\delta m$  includes the mass of the strange current quark, which can be decomposed as

$$\delta m = m_1 \mathbf{1} + m_8 \lambda^8, \quad (7)$$

where  $m_1$  and  $m_8$  represent the singlet and octet components of the current quark masses respectively:  $m_1 = (-\bar{m} + m_s)/3$  and  $m_8 = (\bar{m} - m_s)/\sqrt{3}$ . The Dirac operator (5) with  $\gamma_4$  can be written as

$$\gamma_4 D = -i\partial_4 + h(U(\pi^a)) - \delta m, \quad (8)$$

where  $\partial_4$  stands for the time derivative in Euclidean space.  $h(U)$  is called the one-body Dirac Hamiltonian written as

$$h(U) = i\gamma_4 \gamma_i \partial_i - \gamma_4 M U^{\gamma_5} - \gamma_4 \bar{m}. \quad (9)$$

The presence of the  $\bar{m}$  in the Hamiltonian is required to reproduce correctly the Yukawa tail of the pion field, which plays an essential role in describing the isovector charge radii of the proton [32].

In flavor SU(3), we need to incorporate the hedgehog structure of the pion field [15, 33] by embedding the SU(2)  $U_{\text{SU}(2)}(x)$  field into SU(3) such that the hedgehog symmetry is preserved. The pion field with hedgehog symmetry is expressed as

$$\pi^i = n^i P(r), \quad i = 1, 2, 3, \quad (10)$$

where  $n^i = x^i/r$  with  $r = |\mathbf{x}|$  and  $P(r)$  represents the profile function of the chiral soliton. All other components of  $\pi^a$  are set equal to zero. Thus, to preserve this hedgehog symmetry, the SU(3)  $U(x)$  field can be constructed by the trivial embedding [15]

$$U(x) = \exp(i\pi^a \lambda^a / f_\pi) = \begin{pmatrix} \exp(i\mathbf{n} \cdot \boldsymbol{\tau} P(r)/f_\pi) & 0 \\ 0 & 1 \end{pmatrix}. \quad (11)$$

In the pion mean-field approximation, the pion mean field arises as the solution of the classical equation of motion, which is derived from  $\delta S_{\text{eff}}/\delta P(r) = 0$ . The equation of motion can be solved self-consistently, which resembles the Hartree approximation in many-body problems.

We can derive the matrix elements of the axial-vector current (2) by using the functional integral

$$\begin{aligned} \langle B(p', J'_3) | A_\mu^a(0) | B(p, J_3) \rangle &= \frac{1}{\mathcal{Z}} \lim_{T \rightarrow \infty} \exp \left( ip_4 \frac{T}{2} - ip'_4 \frac{T}{2} \right) \int d^3x d^3y \exp(-i\mathbf{p}' \cdot \mathbf{y} + i\mathbf{p} \cdot \mathbf{x}) \\ &\times \int \mathcal{D}\pi^a \int \mathcal{D}\psi \int \mathcal{D}\psi^\dagger J_B(\mathbf{y}, T/2) \psi^\dagger(0) \gamma_4 \gamma_\mu \gamma_5 \frac{\lambda^a}{2} \psi(0) J_B^\dagger(\mathbf{x}, -T/2) \exp \left[ - \int d^4r \psi^\dagger i D(\pi^a) \psi \right], \end{aligned} \quad (12)$$

where the baryon states  $|B(p, J_3)\rangle$  and  $\langle B(p', J'_3)|$  are respectively written in terms of Ioffe-type baryonic currents

$$\begin{aligned} |B(p, J_3)\rangle &= \lim_{x_4 \rightarrow -\infty} \exp(ip_4 x_4) \frac{1}{\sqrt{\mathcal{Z}}} \int d^3x \exp(i\mathbf{p} \cdot \mathbf{x}) J_B^\dagger(\mathbf{x}, x_4) |0\rangle, \\ \langle B(p', J'_3)| &= \lim_{y_4 \rightarrow \infty} \exp(-ip'_4 y_4) \frac{1}{\sqrt{\mathcal{Z}}} \int d^3y \exp(-i\mathbf{p}' \cdot \mathbf{y}) \langle 0 | J_B(\mathbf{y}, y_4), \end{aligned} \quad (13)$$

where  $J_B(x)$  denotes the Ioffe-type current consisting of  $N_c$  valence quarks [34]

$$J_B(x) = \frac{1}{N_c!} \epsilon_{i_1 \dots i_{N_c}} \Gamma_{JJ_3 TT_3 Y}^{\alpha_1 \dots \alpha_{N_c}} \psi_{\alpha_1 i_1}(x) \dots \psi_{\alpha_{N_c} i_{N_c}}(x), \quad (14)$$

with spin-flavor and color indices  $\alpha_1 \dots \alpha_{N_c}$  and  $i_1 \dots i_{N_c}$ , respectively. The matrices  $\Gamma_{JJ_3 TT_3 Y}^{\alpha_1 \dots \alpha_{N_c}}$  secure the baryon state with pertinent quantum numbers  $JJ_3 TT_3 Y$  by projecting out. Similarly, we can express the creation current operator  $J_B^\dagger(x)$  [11, 35].

In order to quantize the chiral soliton, we have to perform the functional integral over the pNG fields. Since we use the pion mean-field approximation or the saddle-point approximation, we neglect the  $1/N_c$  pion-loop corrections. However, we have to take into account the zero modes that do not change the energy of the soliton. Thus, the functional integral over the  $U$  field is replaced by those over both the rotational and translational zero modes. We refer to Ref. [16] for details. The integral over the translational zero modes yields naturally the Fourier transform,

which indicates that the baryon state has the proper translational symmetry. On the other hand, by performing the rotational zero-mode quantization, we can restore the rotational symmetries. Thus, the zero-mode quantization leads to the collective Hamiltonian

$$H_{\text{coll}} = H_{\text{sym}} + H_{\text{sb}}, \quad (15)$$

where

$$H_{\text{sym}} = M_{\text{cl}} + \frac{1}{2I_1} \sum_{i=1}^3 \hat{J}_i^2 + \frac{1}{2I_2} \sum_{p=4}^7 \hat{J}_p^2, \quad H_{\text{sb}} = \alpha D_{88}^{(8)} + \beta \hat{Y} + \frac{\gamma}{\sqrt{3}} \sum_{i=1}^3 D_{8i}^{(8)} \hat{J}_i. \quad (16)$$

Here,  $I_1$  and  $I_2$  represent the moments of inertia for the soliton and  $D_{ab}^{(8)}$  denote SU(3) Wigner  $D$  functions. The inertial parameters  $\alpha$ ,  $\beta$  and  $\gamma$ , which break flavor SU(3) symmetry explicitly, are expressed in terms of the moments of inertia  $I_1$  and  $I_2$ , and the anomalous moments of inertia  $K_1$  and  $K_2$

$$\alpha = \left( -\frac{\Sigma_{\pi N}}{3\bar{m}} + \frac{K_2}{I_2} \right) m_s, \quad \beta = -\frac{K_2}{I_2} m_s, \quad \gamma = 2 \left( \frac{K_1}{I_1} - \frac{K_2}{I_2} \right) m_s, \quad (17)$$

where  $\Sigma_{\pi N}$  stands for the pion-nucleon  $\Sigma$  term. In the presence of the flavor SU(3) symmetry breaking term  $H_{\text{sb}}$ , the collective wavefunctions of the baryon decuplet are no more in pure states but are mixed with states in higher representations. The states of the baryon decuplet are then obtained by the standard second-order perturbation theory:

$$|B_{10_{3/2}}\rangle = |\mathbf{10}_{3/2}, B\rangle + a_{27}^B |\mathbf{27}_{3/2}, B\rangle + a_{35}^B |\mathbf{35}_{3/2}, B\rangle \quad (18)$$

with the mixing coefficients

$$a_{27}^B = a_{27} \begin{bmatrix} \sqrt{15/2} \\ 2 \\ \sqrt{3/2} \\ 0 \end{bmatrix}, \quad a_{35}^B = a_{35} \begin{bmatrix} 5/\sqrt{14} \\ 2\sqrt{5/7} \\ 3\sqrt{5/14} \\ 2\sqrt{5/7} \end{bmatrix}, \quad (19)$$

respectively, in the basis  $[\Delta, \Sigma^*, \Xi^*, \Omega]$ . The parameters  $a_{27}$  and  $a_{35}$  are written as

$$a_{27} = -\frac{I_2}{8} \left( \alpha + \frac{5}{6}\gamma \right), \quad a_{35} = -\frac{I_2}{24} \left( \alpha - \frac{1}{2}\gamma \right), \quad (20)$$

which have been already determined numerically in Ref. [36]:  $a_{27} = 0.126$  and  $a_{35} = 0.035$ . Each state in Eq. (18) is given in terms of the SU(3) Wigner  $D$  functions in such a way that they satisfy the quantization condition [13].

Having calculated Eq. (12) with the zero-mode quantizations, we can derive the final expressions of the axial-vector form factors

$$g_1^{(0)B}(Q^2) = \frac{\langle \hat{J}_3 \rangle}{3I_1} \{ \mathcal{B}_0^B(Q^2) - \mathcal{B}_2^B(Q^2) \} + \frac{2m_s}{3\sqrt{3}} \langle D_{83}^{(8)} \rangle \left[ \frac{K_1}{I_1} \{ \mathcal{B}_0^B(Q^2) - \mathcal{B}_2^B(Q^2) \} - \{ \mathcal{I}_0^B(Q^2) - \mathcal{I}_2^B(Q^2) \} \right], \quad (21)$$

$$g_3^{(0)B}(Q^2) = \frac{\langle \hat{J}_3 \rangle}{3I_1} \{ \mathcal{B}'_0^B(Q^2) + \mathcal{B}'_2^B(Q^2) \} + \frac{2m_s}{3\sqrt{3}} \langle D_{83}^{(8)} \rangle \left[ \frac{K_1}{I_1} \{ \mathcal{B}'_0^B(Q^2) + \mathcal{B}'_2^B(Q^2) \} - \{ \mathcal{I}'_0^B(Q^2) + \mathcal{I}'_2^B(Q^2) \} \right], \quad (22)$$

for the flavor singlet,

$$\begin{aligned}
g_1^{(a)B}(Q^2) = & \frac{\langle D_{a3}^{(8)} \rangle}{3} \{ \mathcal{A}_0^B(Q^2) - \mathcal{A}_2^B(Q^2) \} + \frac{1}{3\sqrt{3}I_1} \left[ \langle D_{a8}^{(8)} \hat{J}_3 \rangle + \frac{2m_s}{\sqrt{3}} K_1 \langle D_{83}^{(8)} D_{a8}^{(8)} \rangle \right] \{ \mathcal{B}_0^B(Q^2) - \mathcal{B}_2^B(Q^2) \} \\
& + \frac{d_{pq3}}{3I_2} \left[ \langle D_{ap}^{(8)} \hat{J}_q \rangle + \frac{2m_s}{\sqrt{3}} K_2 \langle D_{ap}^{(8)} D_{8q}^{(8)} \rangle \right] \{ \mathcal{C}_0^B(Q^2) - \mathcal{C}_2^B(Q^2) \} - \frac{i\langle D_{a3}^{(8)} \rangle}{6I_1} \{ \mathcal{D}_0^B(Q^2) - \mathcal{D}_2^B(Q^2) \} \\
& + \frac{2m_s}{9} (\langle D_{a3}^{(8)} \rangle - \langle D_{88}^{(8)} D_{a3}^{(8)} \rangle) \{ \mathcal{H}_0^B(Q^2) - \mathcal{H}_2^B(Q^2) \} - \frac{2m_s}{9} \langle D_{83}^{(8)} D_{a8}^{(8)} \rangle \{ \mathcal{I}_0^B(Q^2) - \mathcal{I}_2^B(Q^2) \} \\
& - \frac{2m_s}{3\sqrt{3}} d_{pq3} \langle D_{ap}^{(8)} D_{8q}^{(8)} \rangle \{ \mathcal{J}_0^B(Q^2) - \mathcal{J}_2^B(Q^2) \}, \tag{23}
\end{aligned}$$

$$\begin{aligned}
g_3^{(a)B}(Q^2) = & \frac{\langle D_{a3}^{(8)} \rangle}{3} \{ \mathcal{A}'^B_0(Q^2) + \mathcal{A}'^B_2(Q^2) \} + \frac{1}{3\sqrt{3}I_1} \left[ \langle D_{a8}^{(8)} \hat{J}_3 \rangle + \frac{2m_s}{\sqrt{3}} K_1 \langle D_{83}^{(8)} D_{a8}^{(8)} \rangle \right] \{ \mathcal{B}'^B_0(Q^2) + \mathcal{B}'^B_2(Q^2) \} \\
& + \frac{d_{pq3}}{3I_2} \left[ \langle D_{ap}^{(8)} \hat{J}_q \rangle + \frac{2m_s}{\sqrt{3}} K_2 \langle D_{ap}^{(8)} D_{8q}^{(8)} \rangle \right] \{ \mathcal{C}'^B_0(Q^2) + \mathcal{C}'^B_2(Q^2) \} - \frac{i\langle D_{a3}^{(8)} \rangle}{6I_1} \{ \mathcal{D}'^B_0(Q^2) + \mathcal{D}'^B_2(Q^2) \} \\
& + \frac{2m_s}{9} (\langle D_{a3}^{(8)} \rangle - \langle D_{88}^{(8)} D_{a3}^{(8)} \rangle) \{ \mathcal{H}'^B_0(Q^2) + \mathcal{H}'^B_2(Q^2) \} - \frac{2m_s}{9} \langle D_{83}^{(8)} D_{a8}^{(8)} \rangle \{ \mathcal{I}'^B_0(Q^2) + \mathcal{I}'^B_2(Q^2) \} \\
& - \frac{2m_s}{3\sqrt{3}} d_{pq3} \langle D_{ap}^{(8)} D_{8q}^{(8)} \rangle \{ \mathcal{J}'^B_0(Q^2) + \mathcal{J}'^B_2(Q^2) \}, \tag{24}
\end{aligned}$$

for the non-singlet. The indices  $p$  and  $q$  run over 4 to 7. The  $d_{apq}$  stand for the SU(3) symmetric tensors.  $\mathcal{A}_{0(2)}^B$  to  $\mathcal{J}_{0(2)}^B$  and  $\mathcal{A}'_{0(2)}^B$  to  $\mathcal{J}'_{0(2)}^B$  represent components of the axial-vector form factors, of which the explicit expressions can be found in Appendix A and Ref. [19, 37]. The  $\langle \dots \rangle$  are just the short-handed notations for the matrix elements of the SU(3) Wigner  $D$  function between the decuplet baryons. The explicit results for the matrix elements of the SU(3) Wigner  $D$  function can be found in Appendix B. We have also considered the symmetry-conserving quantization [38], which makes it possible to remove redundant terms by using the limit of the nonrelativistic quark model.

The contributions coming from the flavor SU(3) symmetry breaking consist of two different terms, i.e. that from the effective chiral action and that from the collective wavefunctions, which are decomposed as

$$g_{1(3)}^{(a)B}(Q^2) = (g_{1(3)}^{(a)B}(Q^2))^{(\text{sym})} + (g_{1(3)}^{(a)B}(Q^2))^{(\text{op})} + (g_{1(3)}^{(a)B}(Q^2))^{(\text{wf})}, \tag{25}$$

where  $(g_{1(3)}^{(a)B}(Q^2))^{(\text{sym})}$ ,  $(g_{1(3)}^{(a)B}(Q^2))^{(\text{op})}$ , and  $(g_{1(3)}^{(a)B}(Q^2))^{(\text{wf})}$  correspond respectively to the flavor SU(3) symmetric term, the flavor SU(3) symmetry-breaking term from the effective chiral action and the collective wavefunctions. The singlet axial-vector form factors ( $a = 0$ ) can be written as

$$(g_1^{(0)B}(Q^2))^{(\text{sym})} = \frac{J_3}{3I_1} \{ \mathcal{B}_0^B(Q^2) - \mathcal{B}_2^B(Q^2) \}, \tag{26}$$

$$(g_3^{(0)B}(Q^2))^{(\text{sym})} = \frac{J_3}{3I_1} \{ \mathcal{B}'^B_0(Q^2) + \mathcal{B}'^B_2(Q^2) \}, \tag{27}$$

$$(g_1^{(0)B}(Q^2))^{(\text{op})} = -\frac{m_s Y}{12} \left[ \frac{K_1}{I_1} \{ \mathcal{B}_0^B(Q^2) - \mathcal{B}_2^B(Q^2) \} - \{ \mathcal{I}_0^B(Q^2) - \mathcal{I}_2^B(Q^2) \} \right], \tag{28}$$

$$(g_3^{(0)B}(Q^2))^{(\text{op})} = -\frac{m_s Y}{12} \left[ \frac{K_1}{I_1} \{ \mathcal{B}'^B_0(Q^2) + \mathcal{B}'^B_2(Q^2) \} - \{ \mathcal{I}'^B_0(Q^2) + \mathcal{I}'^B_2(Q^2) \} \right], \tag{29}$$

$$(g_1^{(0)B}(Q^2))^{(\text{wf})} = 0. \tag{30}$$

$$(g_3^{(0)B}(Q^2))^{(\text{wf})} = 0. \tag{31}$$

Note that there are no  $N_c$  leading-order contributions to the singlet axial-vector form factors, which is the well-known fact from any chiral solitonic models. For example, a simple chirally-symmetric version of the Skyrme model yields the null result of  $g_A^{(0)}$  [39]. Since the singlet axial-vector constant of the proton is just its quark spin content, chiral solitonic models explain rather well the reason why the quark spin content of the proton turns out very small experimentally. Moreover, the linear  $m_s$  corrections from the collective wavefunctions also vanish. However, as we will show later explicitly, the linear  $m_s$  corrections contribute most dominantly to the  $g_3^{(0)}(Q^2)$  form factors of the baryon decuplet except for those with hypercharge  $Y = 0$ . As written in Eqs. (26) and (27), the rotational  $1/N_c$  corrections are flavor independent, i.e. they contribute equally to  $g_3^{(0)}(Q^2)$  form factors for any hyperons in the decuplet.

The triplet axial-vector form factors ( $a = 3$ ) are expressed as

$$(g_1^{(3)B}(Q^2))^{(\text{sym})} = -\frac{T_3}{24} \left[ 2\{\mathcal{A}_0^B(Q^2) - \mathcal{A}_2^B(Q^2)\} - \frac{\mathcal{B}_0^B(Q^2) - \mathcal{B}_2^B(Q^2)}{I_1} - \frac{\mathcal{C}_0^B(Q^2) - \mathcal{C}_2^B(Q^2)}{I_2} - \frac{i\{\mathcal{D}_0^B(Q^2) - \mathcal{D}_2^B(Q^2)\}}{I_1} \right], \quad (32)$$

$$(g_3^{(3)B}(Q^2))^{(\text{sym})} = -\frac{T_3}{24} \left[ 2\{\mathcal{A}'_0{}^B(Q^2) + \mathcal{A}'_2{}^B(Q^2)\} - \frac{\mathcal{B}'_0{}^B(Q^2) + \mathcal{B}'_2{}^B(Q^2)}{I_1} - \frac{\mathcal{C}'_0{}^B(Q^2) + \mathcal{C}'_2{}^B(Q^2)}{I_2} - \frac{i\{\mathcal{D}'_0{}^B(Q^2) + \mathcal{D}'_2{}^B(Q^2)\}}{I_1} \right], \quad (33)$$

$$(g_1^{(3)B}(Q^2))^{(\text{op})} = -\frac{m_s T_3}{378} \left[ \begin{pmatrix} 5 \\ 3 \\ 1 \\ 0 \end{pmatrix} \left\{ \frac{K_1}{I_1} \{\mathcal{B}_0^B(Q^2) - \mathcal{B}_2^B(Q^2)\} - \{\mathcal{I}_0^B(Q^2) - \mathcal{I}_2^B(Q^2)\} \right\} \right. \\ \left. + \begin{pmatrix} 11 \\ 15 \\ 19 \\ 0 \end{pmatrix} \left\{ \frac{K_2}{I_2} \{\mathcal{C}_0^B(Q^2) - \mathcal{C}_2^B(Q^2)\} - \{\mathcal{J}_0^B(Q^2) - \mathcal{J}_2^B(Q^2)\} \right\} \right. \\ \left. + \begin{pmatrix} 16 \\ 18 \\ 20 \\ 21 \end{pmatrix} \{\mathcal{H}_0^B(Q^2) - \mathcal{H}_2^B(Q^2)\} \right], \quad (34)$$

$$(g_3^{(3)B}(Q^2))^{(\text{op})} = -\frac{m_s T_3}{378} \left[ \begin{pmatrix} 5 \\ 3 \\ 1 \\ 0 \end{pmatrix} \left\{ \frac{K_1}{I_1} \{\mathcal{B}'_0{}^B(Q^2) + \mathcal{B}'_2{}^B(Q^2)\} - \{\mathcal{I}'_0{}^B(Q^2) + \mathcal{I}'_2{}^B(Q^2)\} \right\} \right. \\ \left. + \begin{pmatrix} 11 \\ 15 \\ 19 \\ 0 \end{pmatrix} \left\{ \frac{K_2}{I_2} \{\mathcal{C}'_0{}^B(Q^2) + \mathcal{C}'_2{}^B(Q^2)\} - \{\mathcal{J}'_0{}^B(Q^2) + \mathcal{J}'_2{}^B(Q^2)\} \right\} \right. \\ \left. + \begin{pmatrix} 16 \\ 18 \\ 20 \\ 21 \end{pmatrix} \{\mathcal{H}'_0{}^B(Q^2) + \mathcal{H}'_2{}^B(Q^2)\} \right], \quad (35)$$

$$(g_1^{(3)B}(Q^2))^{(\text{wf})} = -\frac{T_3}{24} \left[ \frac{a_{27}}{3} \begin{pmatrix} 5 \\ 6 \\ 7 \\ 0 \end{pmatrix} \left\{ 2\{\mathcal{A}_0^B(Q^2) - \mathcal{A}_2^B(Q^2)\} + \frac{3\{\mathcal{B}_0^B(Q^2) - \mathcal{B}_2^B(Q^2)\}}{I_1} + \frac{\mathcal{C}_0^B(Q^2) - \mathcal{C}_2^B(Q^2)}{I_2} - \frac{i\{\mathcal{D}_0^B(Q^2) - \mathcal{D}_2^B(Q^2)\}}{I_1} \right\} \right. \\ \left. + \frac{a_{35}}{7} \begin{pmatrix} 1 \\ 2 \\ 3 \\ 0 \end{pmatrix} \left\{ 2\{\mathcal{A}_0^B(Q^2) - \mathcal{A}_2^B(Q^2)\} - \frac{5\{\mathcal{B}_0^B(Q^2) - \mathcal{B}_2^B(Q^2)\}}{I_1} \right\} \right]$$

$$\left. + \frac{5\{\mathcal{C}_0^B(Q^2) - \mathcal{C}_2^B(Q^2)\}}{I_2} - \frac{i\{\mathcal{D}_0^B(Q^2) - \mathcal{D}_2^B(Q^2)\}}{I_1} \right\} \Bigg], \quad (36)$$

$$\begin{aligned} (g_3^{(3)B}(Q^2))^{(\text{wf})} = & -\frac{T_3}{24} \left[ \frac{a_{27}}{3} \begin{pmatrix} 5 \\ 6 \\ 7 \\ 0 \end{pmatrix} \left\{ 2\{\mathcal{A}_0'^B(Q^2) + \mathcal{A}_2'^B(Q^2)\} + \frac{3\{\mathcal{B}_0'^B(Q^2) + \mathcal{B}_2'^B(Q^2)\}}{I_1} \right. \right. \\ & \left. \left. + \frac{\mathcal{C}_0'^B(Q^2) + \mathcal{C}_2'^B(Q^2)}{I_2} - \frac{i\{\mathcal{D}_0'^B(Q^2) + \mathcal{D}_2'^B(Q^2)\}}{I_1} \right\} \right. \\ & + \frac{a_{35}}{7} \begin{pmatrix} 1 \\ 2 \\ 3 \\ 0 \end{pmatrix} \left\{ 2\{\mathcal{A}_0'^B(Q^2) + \mathcal{A}_2'^B(Q^2)\} - \frac{5\{\mathcal{B}_0'^B(Q^2) + \mathcal{B}_2'^B(Q^2)\}}{I_1} \right. \\ & \left. \left. + \frac{5\{\mathcal{C}_0'^B(Q^2) + \mathcal{C}_2'^B(Q^2)\}}{I_2} - \frac{i\{\mathcal{D}_0'^B(Q^2) + \mathcal{D}_2'^B(Q^2)\}}{I_1} \right\} \right] \Bigg]. \quad (37) \end{aligned}$$

Note that they are proportional to the eigenvalues of the third component of the isospin operator,  $T_3$ . The octet axial-vector form factors ( $a = 8$ ) are obtained as

$$(g_1^{(8)B}(Q^2))^{(\text{sym})} = -\frac{Y}{16\sqrt{3}} \left[ 2\{\mathcal{A}_0^B(Q^2) - \mathcal{A}_2^B(Q^2)\} - \frac{\mathcal{B}_0^B(Q^2) - \mathcal{B}_2^B(Q^2)}{I_1} - \frac{\mathcal{C}_0^B(Q^2) - \mathcal{C}_2^B(Q^2)}{I_2} - \frac{i\{\mathcal{D}_0^B(Q^2) - \mathcal{D}_2^B(Q^2)\}}{I_1} \right], \quad (38)$$

$$(g_3^{(8)B}(Q^2))^{(\text{sym})} = -\frac{Y}{16\sqrt{3}} \left[ 2\{\mathcal{A}_0'^B(Q^2) + \mathcal{A}_2'^B(Q^2)\} - \frac{\mathcal{B}_0'^B(Q^2) + \mathcal{B}_2'^B(Q^2)}{I_1} - \frac{\mathcal{C}_0'^B(Q^2) + \mathcal{C}_2'^B(Q^2)}{I_2} - \frac{i\{\mathcal{D}_0'^B(Q^2) + \mathcal{D}_2'^B(Q^2)\}}{I_1} \right], \quad (39)$$

$$\begin{aligned} (g_1^{(8)B}(Q^2))^{(\text{op})} = & \frac{m_s}{252\sqrt{3}} \left[ \begin{pmatrix} 3 \\ 2 \\ -3 \\ -12 \end{pmatrix} \left\{ \frac{K_1}{I_1} \{\mathcal{B}_0^B(Q^2) - \mathcal{B}_2^B(Q^2)\} - \{\mathcal{I}_0^B(Q^2) - \mathcal{I}_2^B(Q^2)\} \right\} \right. \\ & + \begin{pmatrix} 15 \\ -4 \\ -15 \\ -18 \end{pmatrix} \left\{ \frac{K_2}{I_2} \{\mathcal{C}_0^B(Q^2) - \mathcal{C}_2^B(Q^2)\} - \{\mathcal{J}_0^B(Q^2) - \mathcal{J}_2^B(Q^2)\} \right\} \\ & \left. - 2 \begin{pmatrix} 12 \\ 1 \\ -12 \\ -27 \end{pmatrix} \{\mathcal{H}_0^B(Q^2) - \mathcal{H}_2^B(Q^2)\} \right], \quad (40) \end{aligned}$$

$$\begin{aligned} (g_3^{(8)B}(Q^2))^{(\text{op})} = & \frac{m_s}{252\sqrt{3}} \left[ \begin{pmatrix} 3 \\ 2 \\ -3 \\ -12 \end{pmatrix} \left( \frac{K_1}{I_1} \{\mathcal{B}_0'^B(Q^2) + \mathcal{B}_2'^B(Q^2)\} - \{\mathcal{I}_0'^B(Q^2) + \mathcal{I}_2'^B(Q^2)\} \right) \right. \\ & + \begin{pmatrix} 15 \\ -4 \\ -15 \\ -18 \end{pmatrix} \left( \frac{K_2}{I_2} \{\mathcal{C}_0'^B(Q^2) + \mathcal{C}_2'^B(Q^2)\} - \{\mathcal{J}_0'^B(Q^2) + \mathcal{J}_2'^B(Q^2)\} \right) \\ & \left. - 2 \begin{pmatrix} 12 \\ 1 \\ -12 \\ -27 \end{pmatrix} \{\mathcal{H}_0'^B(Q^2) + \mathcal{H}_2'^B(Q^2)\} \right], \quad (41) \end{aligned}$$



$$\begin{aligned}
(g_1^{(8)B}(Q^2))^{(\text{wf})} = & \frac{1}{16\sqrt{3}} \left[ \frac{a_{27}}{3} \begin{pmatrix} 15 \\ 8 \\ 3 \\ 0 \end{pmatrix} \left\{ 2\{\mathcal{A}_0^B(Q^2) - \mathcal{A}_2^B(Q^2)\} + \frac{3\{\mathcal{B}_0^B(Q^2) - \mathcal{B}_2^B(Q^2)\}}{I_1} \right. \right. \\
& \left. \left. + \frac{\mathcal{C}_0^B(Q^2) - \mathcal{C}_2^B(Q^2)}{I_2} - \frac{i\{\mathcal{D}_0^B(Q^2) - \mathcal{D}_2^B(Q^2)\}}{I_1} \right\} \right. \\
& \left. - \frac{a_{35}}{7} \begin{pmatrix} 5 \\ 8 \\ 9 \\ 8 \end{pmatrix} \left\{ 2\{\mathcal{A}_0^B(Q^2) - \mathcal{A}_2^B(Q^2)\} - \frac{5\{\mathcal{B}_0^B(Q^2) - \mathcal{B}_2^B(Q^2)\}}{I_1} \right. \right. \\
& \left. \left. + \frac{5\{\mathcal{C}_0^B(Q^2) - \mathcal{C}_2^B(Q^2)\}}{I_2} - \frac{i\{\mathcal{D}_0^B(Q^2) - \mathcal{D}_2^B(Q^2)\}}{I_1} \right\} \right], \tag{42}
\end{aligned}$$

$$\begin{aligned}
(g_3^{(8)B}(Q^2))^{(\text{wf})} = & \frac{1}{16\sqrt{3}} \left[ \frac{a_{27}}{3} \begin{pmatrix} 15 \\ 8 \\ 3 \\ 0 \end{pmatrix} \left\{ 2\{\mathcal{A}_0'^B(Q^2) + \mathcal{A}_2'^B(Q^2)\} + \frac{3\{\mathcal{B}_0'^B(Q^2) + \mathcal{B}_2'^B(Q^2)\}}{I_1} \right. \right. \\
& \left. \left. + \frac{\mathcal{C}_0'^B(Q^2) + \mathcal{C}_2'^B(Q^2)}{I_2} - \frac{i\{\mathcal{D}_0'^B(Q^2) + \mathcal{D}_2'^B(Q^2)\}}{I_1} \right\} \right. \\
& \left. - \frac{a_{35}}{7} \begin{pmatrix} 5 \\ 8 \\ 9 \\ 8 \end{pmatrix} \left\{ 2\{\mathcal{A}_0'^B(Q^2) + \mathcal{A}_2'^B(Q^2)\} - \frac{5\{\mathcal{B}_0'^B(Q^2) + \mathcal{B}_2'^B(Q^2)\}}{I_1} \right. \right. \\
& \left. \left. + \frac{5\{\mathcal{C}_0'^B(Q^2) + \mathcal{C}_2'^B(Q^2)\}}{I_2} - \frac{i\{\mathcal{D}_0'^B(Q^2) + \mathcal{D}_2'^B(Q^2)\}}{I_1} \right\} \right]. \tag{43}
\end{aligned}$$

#### IV. RESULTS AND DISCUSSION

In the  $\chi$ QSM, the only free parameter is the dynamical quark mass,  $M$ . Though it is determined by the saddle-point approximation from the instanton vacuum, it is fixed by reproducing the electric form factor of the proton. The pion decay constant is determined by using the experimental data  $f_\pi = 93$  MeV. The current-quark masses are fixed by the pion and kaon masses. However, we will take the value of the strange current quark mass to be  $m_s = 180$  MeV that is larger than those taken in chiral perturbation theory. The reason is that with this value of 180 MeV we are able to reproduce the mass splittings of the hyperons and singly heavy baryons. Thus, we have no free parameter to fit in the present calculation.

Since there are numerous form factors of the baryon decuplet, we will first concentrate on those of the  $\Delta^+$  isobar and  $\Omega^-$  hyperon. In the left panel of Fig. 1, we draw the results of the triplet axial-vector form factor  $g_1^{(3)}(Q^2)$  of the  $\Delta^+$  whereas in the right panel we show those of  $g_3^{(3)}(Q^2)$ . As for those for other members of the baryon decuplet, we will display them on Fig. 5 and Fig. 6 and will discuss them later on. Note that as defined in Eq. (2)  $g_1^{(3)}(Q^2)$  form factor is the most well-known axial-vector form factor. A great deal of theoretical works have considered this one, because its value at  $Q^2 = 0$  gives the axial charge of the  $\Delta^+$ . The Goldberger-Treiman relation connects it to the strong coupling constant  $g_{\pi\Delta\Delta}$ . As depicted in the left panel of Fig. 1, the results of  $g_1^{(3)}(Q^2)$  decrease monotonically and slowly as  $Q^2$  increases. The effects of the linear  $m_s$  corrections are marginal. They provide approximately overall 10 % correction to the form factor  $g_1^{(3)}(Q^2)$ . The right panel of Fig. 1 exhibits the numerical results for the second axial-vector form factor  $g_3^{(3)}(Q^2)$  of the  $\Delta^+$ . In contrast with  $g_1^{(3)}(Q^2)$ , the  $Q^2$  dependence of  $g_3^{(3)}(Q^2)$  is prominent. The result of  $g_3^{(3)}(Q^2)$  falls off drastically as  $Q^2$  increases. One can understand this behavior as follows: as shown in Appendix A, all components of  $g_3^{(3)}(Q^2)$  are proportional to  $Q^{-2}$ , which cause such strong  $Q^2$  dependence. Moreover, the kinematical prefactor makes the magnitude of  $g_3^{(3)}(Q^2)$  much larger than that of  $g_1^{(3)}(Q^2)$ . On the other hand, the effects of flavor SU(3) symmetry breaking are rather small on  $g_3^{(3)}(Q^2)$ .

In Fig. 2, we show the results of the singlet axial-vector form factors. As shown in the left panel of Fig. 2, the effects of the linear  $m_s$  are almost negligible on the  $g_1^{(0)}(Q^2)$  form factors of both  $\Delta^+$  and  $\Omega^-$ . Note that the singlet axial-vector constant,  $g_1^{(0)B}(0)$ , explains the quark spin content of the corresponding baryon. If one neglects the

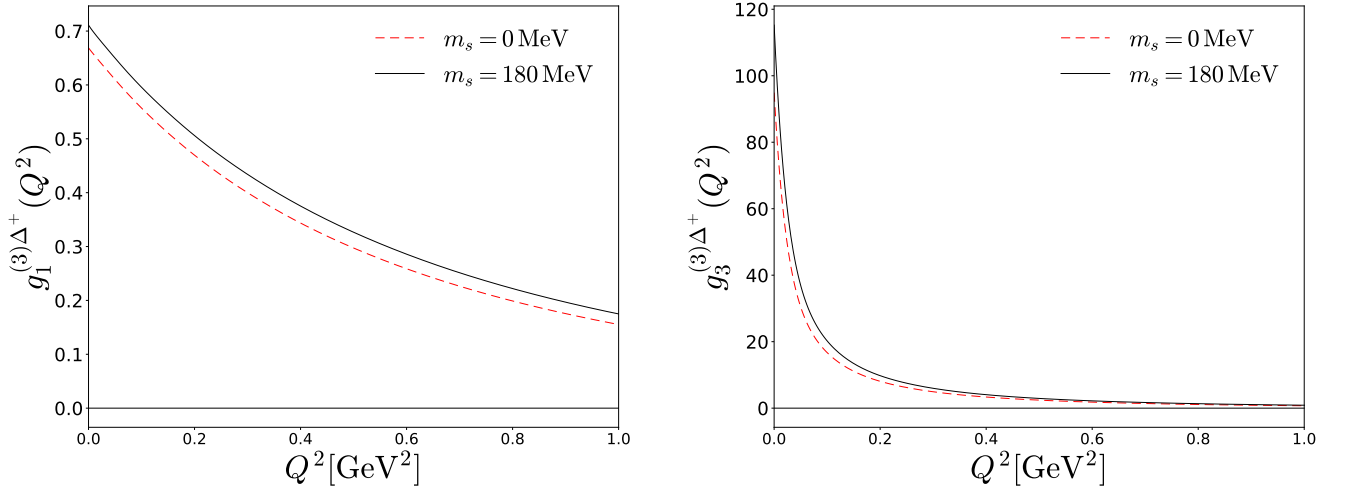


FIG. 1. Effects of the explicit flavor SU(3) symmetry breaking on the triplet axial-vector form factors  $g_1^{(3)}(Q^2)$  and  $g_3^{(3)}(Q^2)$  of the  $\Delta^+$  isobar. In the right panel, the results of  $g_1^{(3)}(Q^2)$  are drawn whereas in the left panel, those of  $g_3^{(3)}(Q^2)$  are depicted. The solid and dashed curves represent the total results and those in the SU(3) symmetric case, respectively.

effects of flavor SU(3) symmetry breaking,  $g_1^{(0)B}(Q^2)$  is independent of the flavor content of a decuplet baryon, as explicitly expressed in Eq. (26).  $g_3^{(0)B}(Q^2)$  is also flavor-independent (see Eq. (27)) without  $m_s$  corrections. However, when it comes to the  $g_3^{(0)}(Q^2)$  form factors, the linear  $m_s$  corrections contribute remarkably large to them. This can be understood by scrutinizing Eq. (25) for the singlet axial-vector form factors, i.e. when  $a = 0$ . The flavor SU(3) symmetric part  $(g_3^{(0)B}(Q^2))^{(\text{sym})}$  contains only the rotational  $1/N_c$  corrections. Since there are no wavefunction corrections, we have only the linear  $m_s$  corrections from the current quark mass term of the effective chiral action. The tensor contribution  $\mathcal{I}_2^B(Q^2)$  is the most dominant one that governs the behavior of  $g_3^{(0)\Delta^+}(Q^2)$ . Even though we ignore all other terms, the result is not much changed. If one looks into the expression for  $\mathcal{I}_2^B(Q^2)$ , which is given in Appendix A, one can easily see that in general the tensor contributions are dominant over the scalar ones kinematically. We can find a similar tendency in the  $\Omega^-$  singlet axial-vector form factors as shown in the lower panel of Fig. 2. In the case of  $\Omega^-$ , the results of  $g_1^{(0)}(Q^2)$  are very similar to those of  $\Delta^+$ . The rotational  $1/N_c$  corrections give the positive values of  $g_3^{(0)}(Q^2)$  for  $\Omega^-$ , which are the same as in the case of  $\Delta^+$ . This is due to the fact that as explained previously, the rotational  $1/N_c$  corrections do not depend on the flavor of the baryon decuplet. On the other hand, the linear  $m_s$  contributions become negative to the  $g_3^{(0)\Omega^-}(Q^2)$  form factor. This is due to the fact that the hypercharge is present in Eq. (29). One could suspect that the second-order  $m_s$  corrections might come into play in describing the  $g_3^{(0)}(Q^2)$  form factors of the baryon decuplet. However, the second-order  $m_s$  corrections should be suppressed at least by two reasons: Firstly, the parameter  $(m_s/\Lambda)^2$  is much smaller than the leading term, where  $\Lambda$  is the cutoff mass or the normalization scale of the  $\chi$ QSM, which is of order 1 GeV. Secondly, expressions for the second-order  $m_s$  corrections contain doubly-summed energy denominators, which lead to further suppression. So, we expect that the second-order  $m_s$  corrections should be much smaller than the linear  $m_s$  corrections.

Figure 3 depicts the octet axial-vector form factors of  $\Delta^+$  and  $\Omega^-$ . As illustrated in the upper left panel of Fig. 3, the linear  $m_s$  corrections suppress  $g_1^{(8)\Delta^+}(Q^2)$  by about 17 %, while they are negligible to  $g_1^{(8)\Omega^-}(Q^2)$  as shown in the lower left panel of fig. 3. Interestingly, the linear  $m_s$  corrections to  $g_1^{(8)\Omega^-}(Q^2)$  become visible as  $Q^2$  increases, though they are still very small. On the other hand, the results for  $g_3^{(8)\Delta^+}(Q^2)$  show peculiar behavior. While it shows a similar tendency of the linear  $m_s$  corrections to  $g_1^{(8)\Delta^+}(Q^2)$ , their magnitude is rather large. Interestingly, the wavefunction corrections come into play in this case. As shown in Eq. (43), the contribution from the 27-plet to  $g_3^{(8)\Delta^+}(Q^2)$  dominates over all other contributions, since it contains  $\mathcal{A}_2^{\prime\Delta^+}(Q^2)$  and  $i\mathcal{D}_2^{\prime\Delta^+}(Q^2)$ , which are the most contributive ones. The linear  $m_s$  corrections arising from the effective chiral action are much smaller than those of the wavefunction corrections. As a result, the  $g_3^{(8)\Delta^+}(Q^2)$  form factor is much reduced by the effects of flavor SU(3) symmetry breaking. The lower right panel of Fig. 3 draws the numerical results for  $g_3^{(8)\Omega^-}(Q^2)$ . In contrast to the  $g_3^{(8)\Delta^+}(Q^2)$ , the linear  $m_s$  corrections are almost negligible. The reason can be also found in Eq. (43), where the

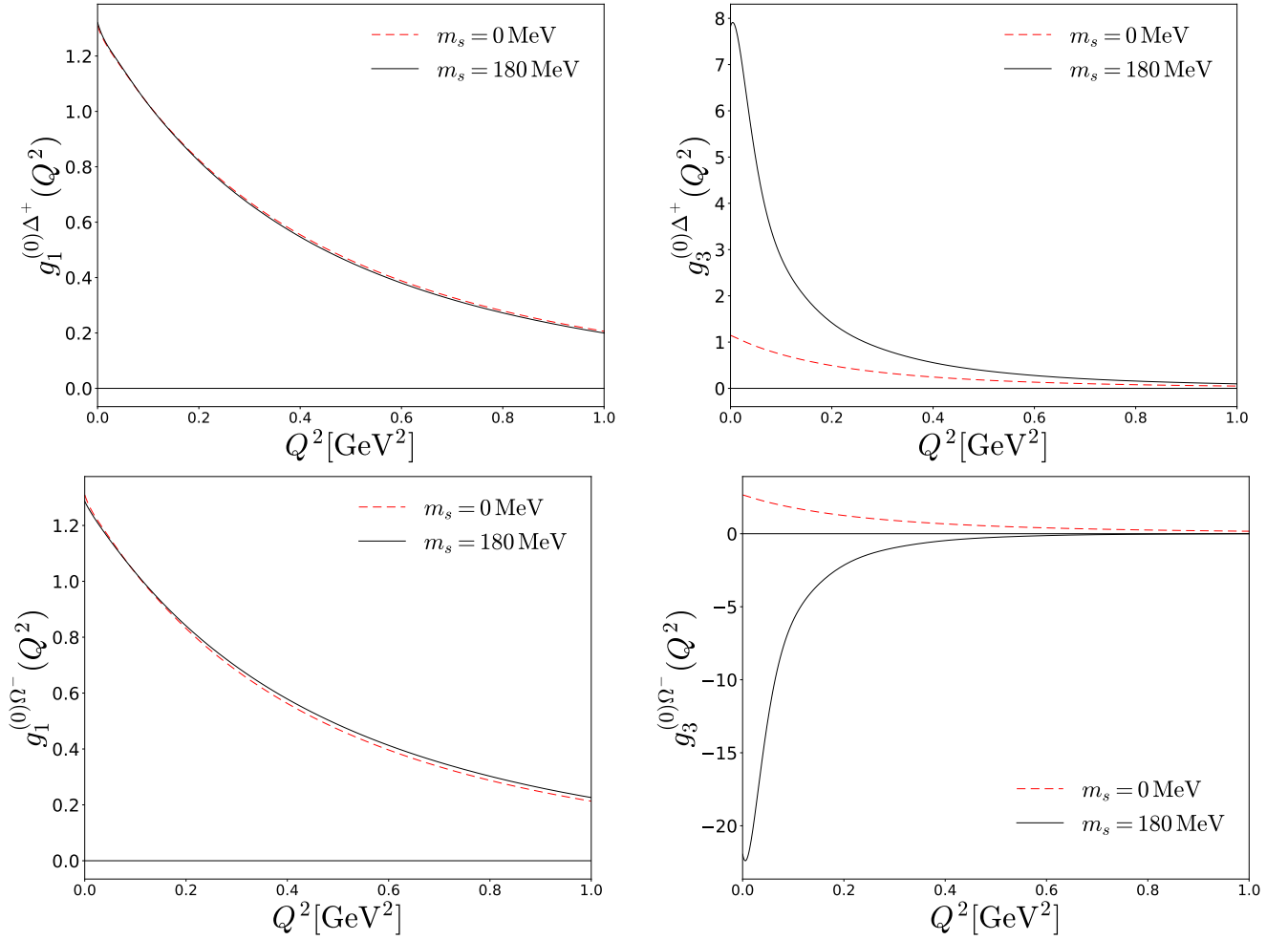


FIG. 2. Effects of the explicit flavor SU(3) symmetry breaking on the singlet axial-vector form factors  $g_1^{(3)}(Q^2)$  and  $g_3^{(3)}(Q^2)$  of the  $\Delta^+$  isobar and  $\Omega^-$ . In the upper right panel, the results of  $g_1^{(0)}(Q^2)$  of  $\Delta^+$  are drawn whereas in the upper left panel, those of  $g_3^{(0)\Delta^+}(Q^2)$  are depicted. The lower left panel shows the results of the first  $\Omega^-$  singlet axial-vector form factor  $g_1^{(0)}(Q^2)$ , while the lower right one illustrates those of the  $g_3^{(0)\Omega^-}(Q^2)$ . The solid and dashed curves represent the total results and those in the SU(3) symmetric case, respectively. Notations are the same as in Fig. 1.

contribution of the 27-plet vanishes.

Since there are only the results from lattice QCD on the triplet axial-vector form factors of the  $\Delta^+$  [3], it is of great importance to compare the present results with them. However, before we make a comparison of the present results with the lattice data, we have to consider the unphysical pion mass used in the lattice simulation [3]. This means that we need to derive the profile function of the chiral soliton by solving the equation of motion again. This can be done as follows: In Eq. (9), we replace the physical value of the average current quark mass of the up and down quarks with the unphysical one that corresponds to the pion mass adopted by the lattice calculation. Then the axial-vector form factors of the baryon decuplet can be recalculated by using the profile function with the unphysical value of the pion mass. In fact, the pion mass dependence of baryonic observables has been already investigated [26, 27, 40, 41] in the context of the comparison with lattice results.

In Fig. 4, we exhibit the results of the  $\Delta^+$  triplet axial-vector form factors in comparison with those from the lattice calculation, taking into account the values of the unphysical pion mass, which are used in Ref. [3]. As mentioned previously,  $h_1^{(3)}(Q^2)$  and  $h_3^{(3)}(Q^2)$  are in effect the same respectively as  $g_1^{(3)}(Q^2)$  and  $g_3^{(3)}(Q^2)$  except for the kinematical factors, which have been expressed implicitly in Eq. (3). As depicted in the upper left panel of Fig. 4, the results of  $g_1^{(3)\Delta^+}(Q^2)$  increase as larger values of the unphysical pion mass are used. The  $Q^2$  dependence of the form factor tends to be similar to that of the lattice calculation. However, the lattice data seem to fall off rather slowly as  $Q^2$  increases, compared with the present results. The upper right panel of Fig. 4 depicts the results for  $g_3^{(3)\Delta^+}(Q^2)$  with

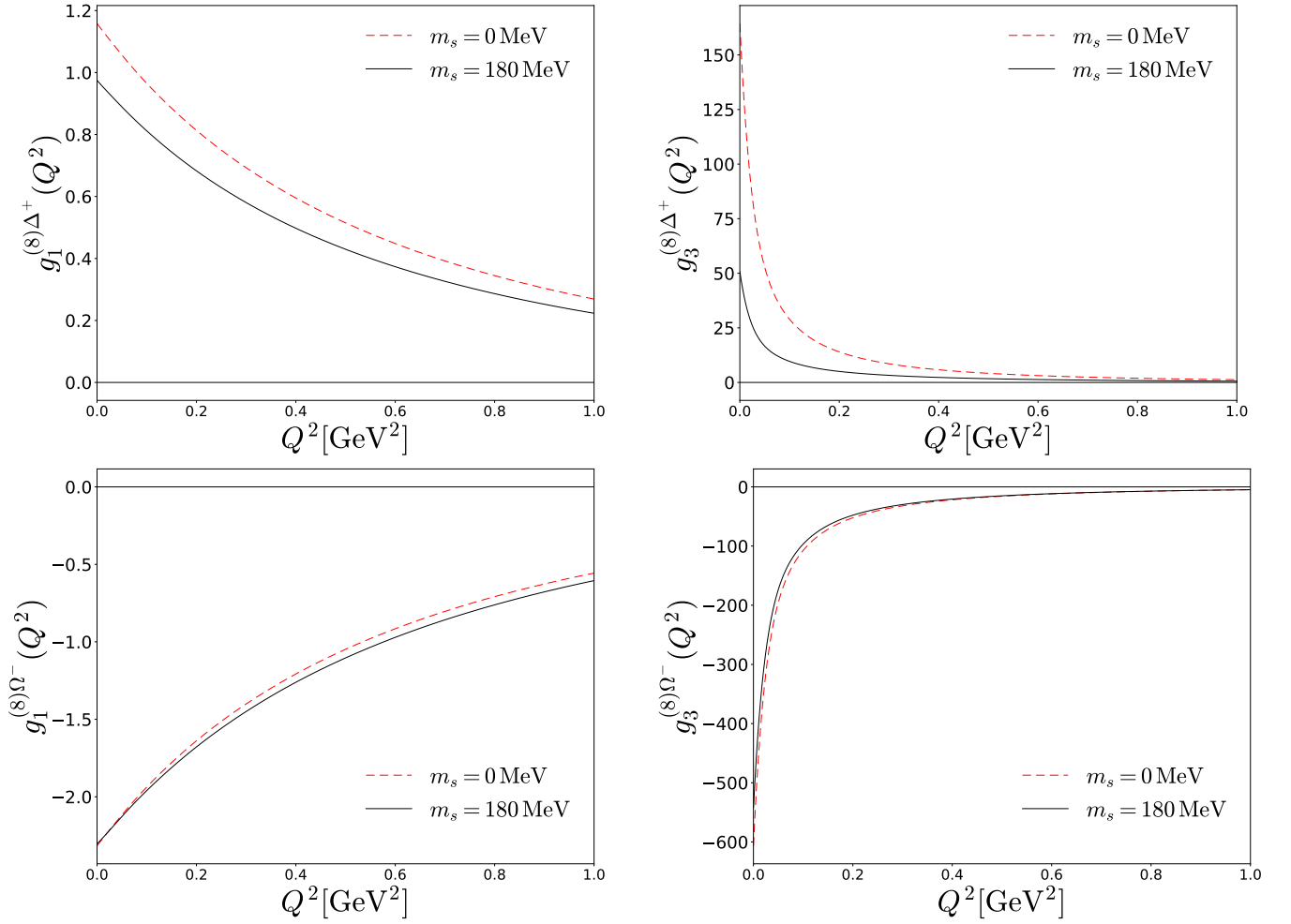


FIG. 3. Effects of the explicit flavor SU(3) symmetry breaking on the octet axial-vector form factors of the  $\Delta^+$  and  $\Omega^-$  baryon. Notations are the same as in Fig. 1.

the pion mass varied. It is interesting to see that the magnitude of the form factor decreases as large pion masses are employed. The lattice data on  $g_3^{(3)\Delta^+}(Q^2)$  show relatively smaller fluctuations, compared with those on other axial-vector form factors. The  $Q^2$  dependence of the present results is in line with the lattice data. Since there are large uncertainties in the lattice results and a lack of data in smaller  $Q^2$  regions, it is rather difficult to make a clear comparison of the present results with those of the lattice calculation. In the lower panel of Fig. 4, we compare the results of  $h_1^{(3)\Delta^+}(Q^2)$  and  $h_3^{(3)\Delta^+}(Q^2)$  with those of lattice QCD. Since the lattice data show large fluctuations in general, we are not able to draw any meaningful conclusions.

In Fig. 5, we show the numerical results for the triplet axial-vector form factors  $g_1^{(3)}(Q^2)$  of the baryon decuplet except for  $\Delta^+$  and  $\Omega^-$ . The effects of the flavor SU(3) symmetry breaking are in general marginal. Figure 6 presents those for  $g_3^{(3)}(Q^2)$  of all other members of the decuplet. The tendency of the linear  $m_s$  corrections is basically the same as that for  $\Delta^+$  as discussed in Fig. 1. In Fig. 7 we illustrate those for the singlet axial-vector form factors  $g_1^{(0)}(Q^2)$  for the other members of the decuplet. Again the results look very similar to those of  $\Delta^+$  and  $\Omega^-$  as explained in Fig. 2. As mentioned previously, if one neglects the effects of flavor SU(3) symmetry breaking, then  $g_1^{(0)B}(Q^2)$  is flavor-independent as clearly shown in Fig. 7. In Fig. 8 we display the results for the  $g_3^{(0)}(Q^2)$  of the baryon decuplet except for the  $\Delta^+$  and  $\Omega^-$ . In particular, those of  $\Sigma^*$  do not acquire any contributions from the linear  $m_s$  corrections. This can be easily understood by examining Eqs. (29) and (31). Since  $\Sigma^*$  has hypercharge  $Y = 0$ , the linear  $m_s$  corrections from the effective chiral action vanish. The wavefunction corrections do not exist at all for both  $g_1^{(0)}(Q^2)$  and  $g_3^{(0)}(Q^2)$ . Figures 9 and 10 depict respectively the results for  $g_1^{(8)}(Q^2)$  and  $g_3^{(8)}(Q^2)$  for the other members of the baryon decuplet again except for  $\Delta^+$  and  $\Omega^-$ . Interestingly, there are no flavor SU(3) symmetric contributions to

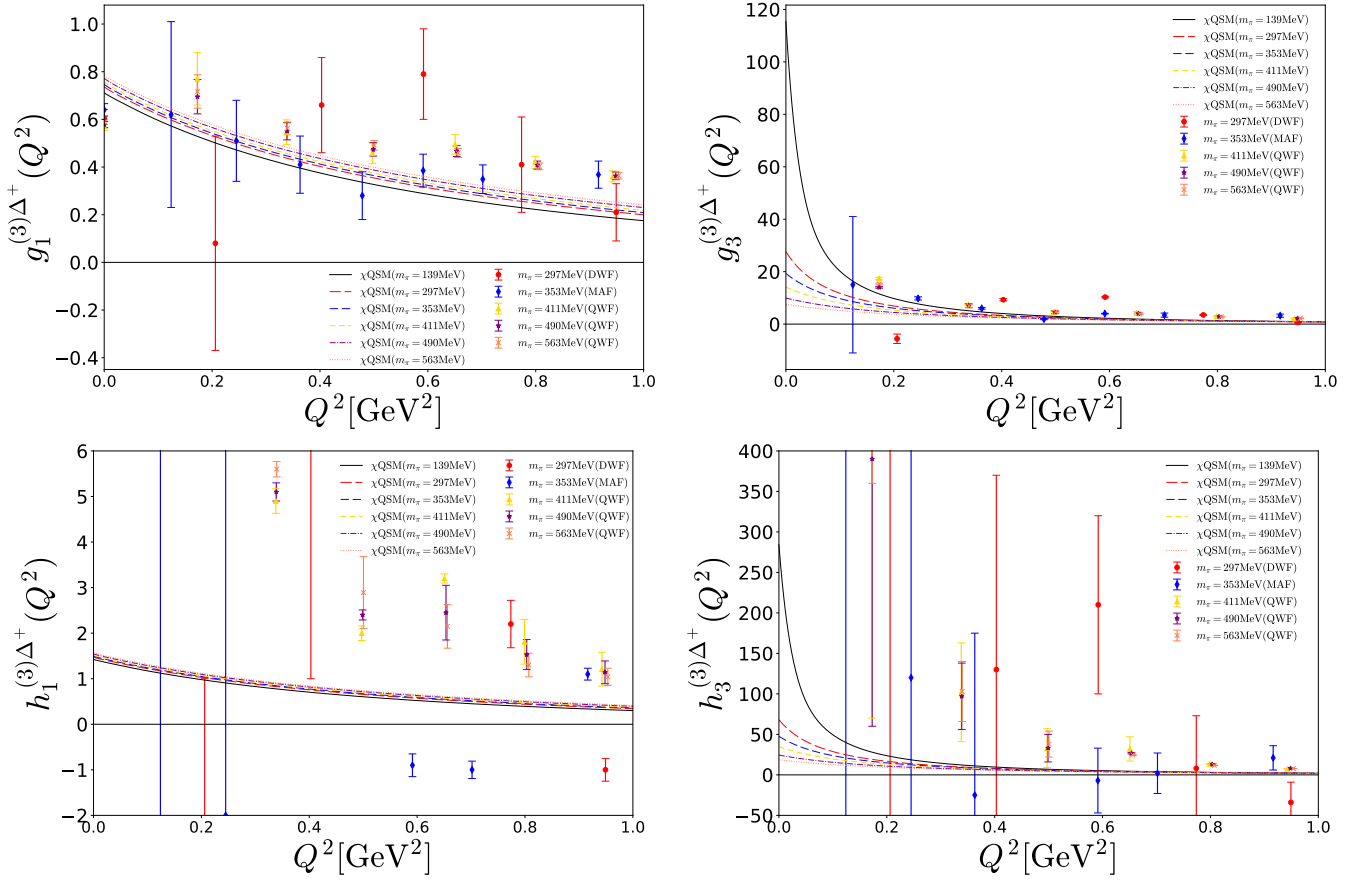


FIG. 4. Numerical results of the triplet axial-vector form factors of the  $\Delta^+$  baryon in comparison with the data taken from lattice QCD [3].

$g_1^{(8)}(Q^2)$  and  $g_3^{(8)}(Q^2)$  of  $\Sigma^*$  because of the hypercharge of  $\Sigma^*$ , as shown in Eqs. (38) and (39). Thus, the linear  $m_s$  corrections are considered to be the leading-order contributions.

In Table I, we list the results for the triplet axial-vector constant, i.e. axial charge with the pion mass varied, intending to compare them with those from lattice QCD [3, 4]. The third row presents the final results from this work with the value of the physical pion mass and the strange quark mass  $m_s = 180$  MeV, whereas the second row gives those without linear  $m_s$  corrections. The present value of the  $\Delta^{++}$  axial charge is in good agreement with those from the RCQM and  $\chi$ PT. However, it is rather difficult to compare the present results with those from lattice QCD. Interestingly, the present results for the triplet axial-vector constants of the other members of the baryon decuplet are in better agreement with the corresponding lattice data. Note that the lattice data are consistently smaller than the values obtained in the present work. Those of  $\Sigma^{*+}$  and  $\Xi^{*0}$  from the RCQM are in very good agreement with the present results.

In Figs. 11 and 12, we show respectively the numerical results for the triplet axial-vector constants of the  $\Delta$  isobars,  $\Sigma^*$  and  $\Xi^*$  as functions of the pion mass, compared them with the lattice data. The magnitudes of  $g_1^{(3)B}(0)$  generally increase as the value of  $m_\pi$  increases. The present results turn out larger than those of lattice QCD. Figure 13 depicts the numerical results for the singlet axial-vector constants of the baryon decuplet as functions of the pion mass in comparison with the lattice data [4]. As we have mentioned already, the values of  $g_1^{(0)B}(0)$  of the baryon decuplet are almost the same each other. As the pion mass grows larger, the magnitudes of  $g_1^{(0)B}(0)$  monotonically increase. When  $m_\pi = 432$  MeV is used, those of  $g_1^{(0)B}(0)$  become larger by about 30 %. Interestingly, the present results get closer to the lattice data as the value of the pion mass increases. They are in very good agreement with the lattice data at  $m_\pi = 432$  MeV. Note that in the present framework the singlet axial-vector constants are isospin symmetric. In Fig. 14, we compare the results for the octet axial-vector constants of the baryon decuplet with the corresponding lattice data with the pion mass varied. Again, the magnitudes of the octet axial-vector constants also rise as the pion mass increases as in the case of  $g_1^{(0)B}(0)$ . However, when we compare the present results with the lattice data, the

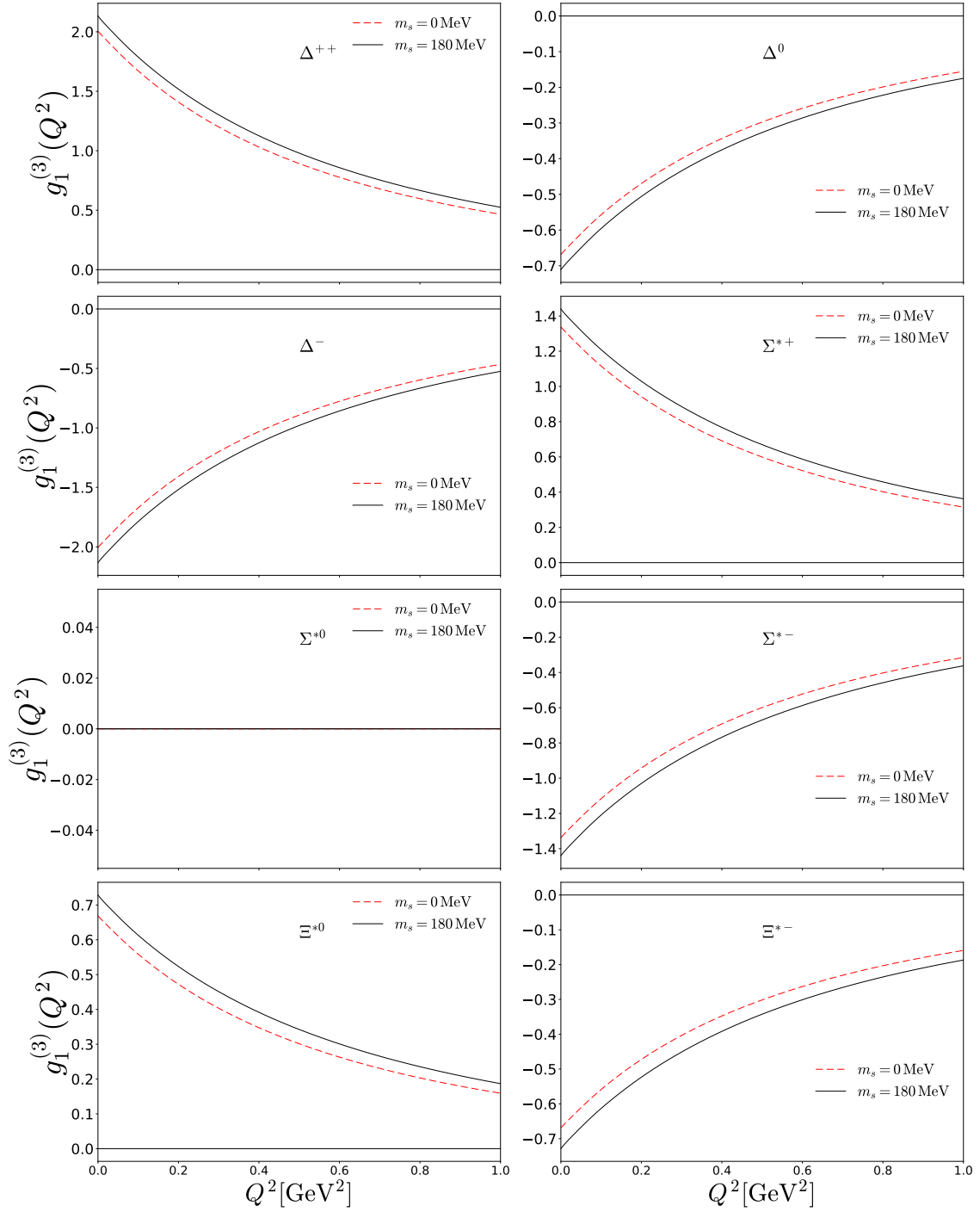


FIG. 5. Effects of the explicit flavor SU(3) symmetry breaking on  $g_1^{(3)B}(Q^2)$  of the baryon decuplet except for the  $\Delta^+$  and  $\Omega^-$  baryons. Notations are the same as in Fig. 1.

situation turns out opposite. That is, the present results tend generally to deviate, except for the  $\Sigma^*$ , from the lattice ones as the pion mass increases. When it comes to the case of  $\Sigma^*$ ,  $g_1^{(8)\Sigma^*}(0)$  exhibits dependence on  $m_\pi$  similar to the corresponding lattice one. The results for  $g_1^{(8)B}(0)$  are in good agreement with the lattice data at  $m_\pi = 213$  MeV.

Table II lists the numerical results for  $g_3^{(3)B}(0)$ ,  $g_3^{(0)B}(0)$  and  $g_3^{(8)B}(0)$ , respectively, from the second row till the fourth row. Since there are no lattice data and no results from other works, they are the very first results for the second set of the axial-vector constants. The fifth row lists the results for the axial radii, which can be derived from

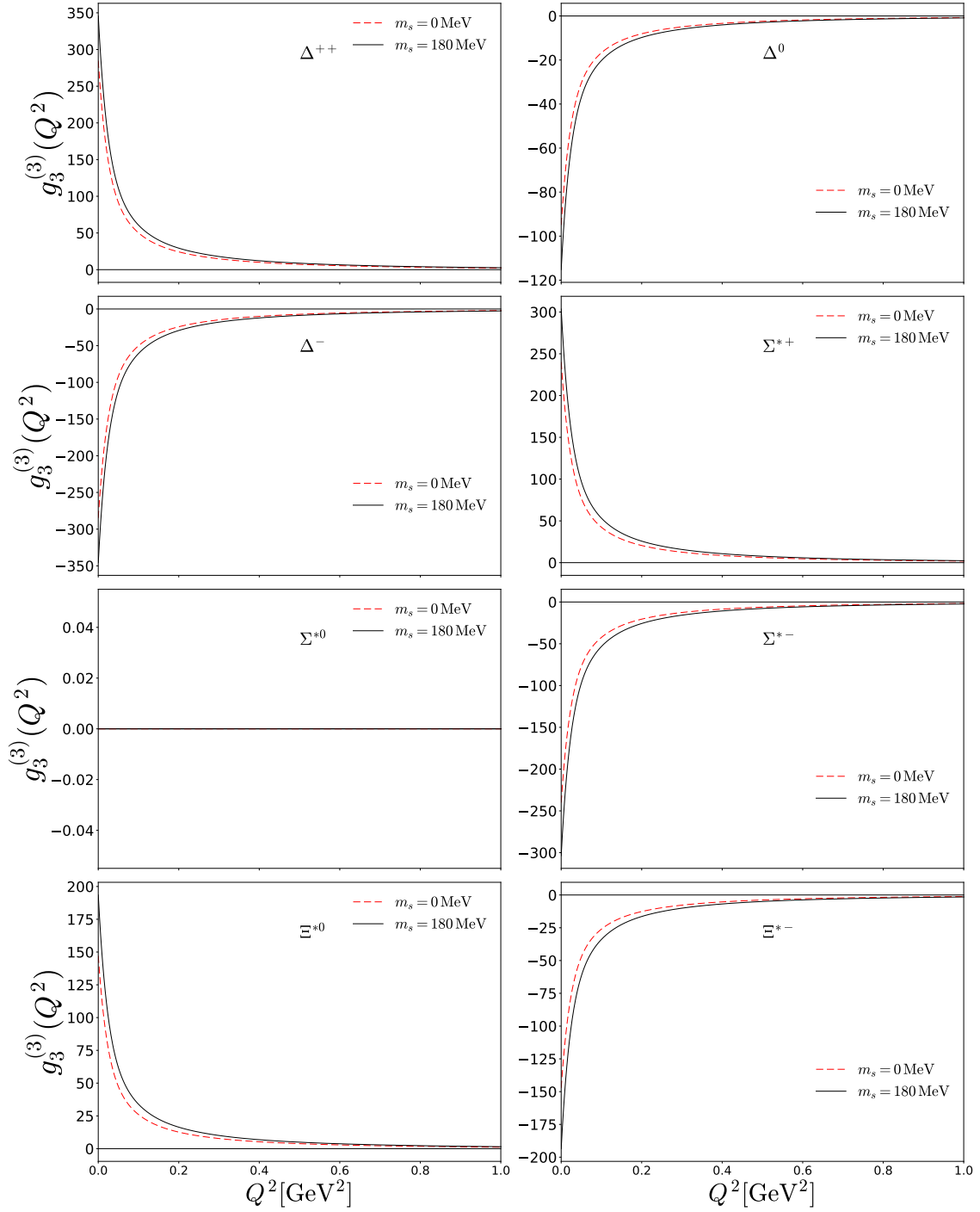


FIG. 6. Effects of the explicit flavor SU(3) symmetry breaking on  $g_3^{(3)B}(Q^2)$  of the baryon decuplet except for the  $\Delta^+$  and  $\Omega^-$  baryons. Notations are the same as in Fig. 1.

the results for the triplet axial-vector form factors of the baryon decuplet as follows

$$\langle r_A^2 \rangle_B = \frac{-6}{g_1^{(3)B}(0)} \left. \frac{\partial g_1^{(3)B}(Q^2)}{\partial Q^2} \right|_{Q^2=0}. \quad (44)$$

Note that when the strangeness of a decuplet baryon increases, the value of the axial radius becomes smaller, as shown in Table II. This can be understood, since the corresponding mass becomes larger due to the strange-quark

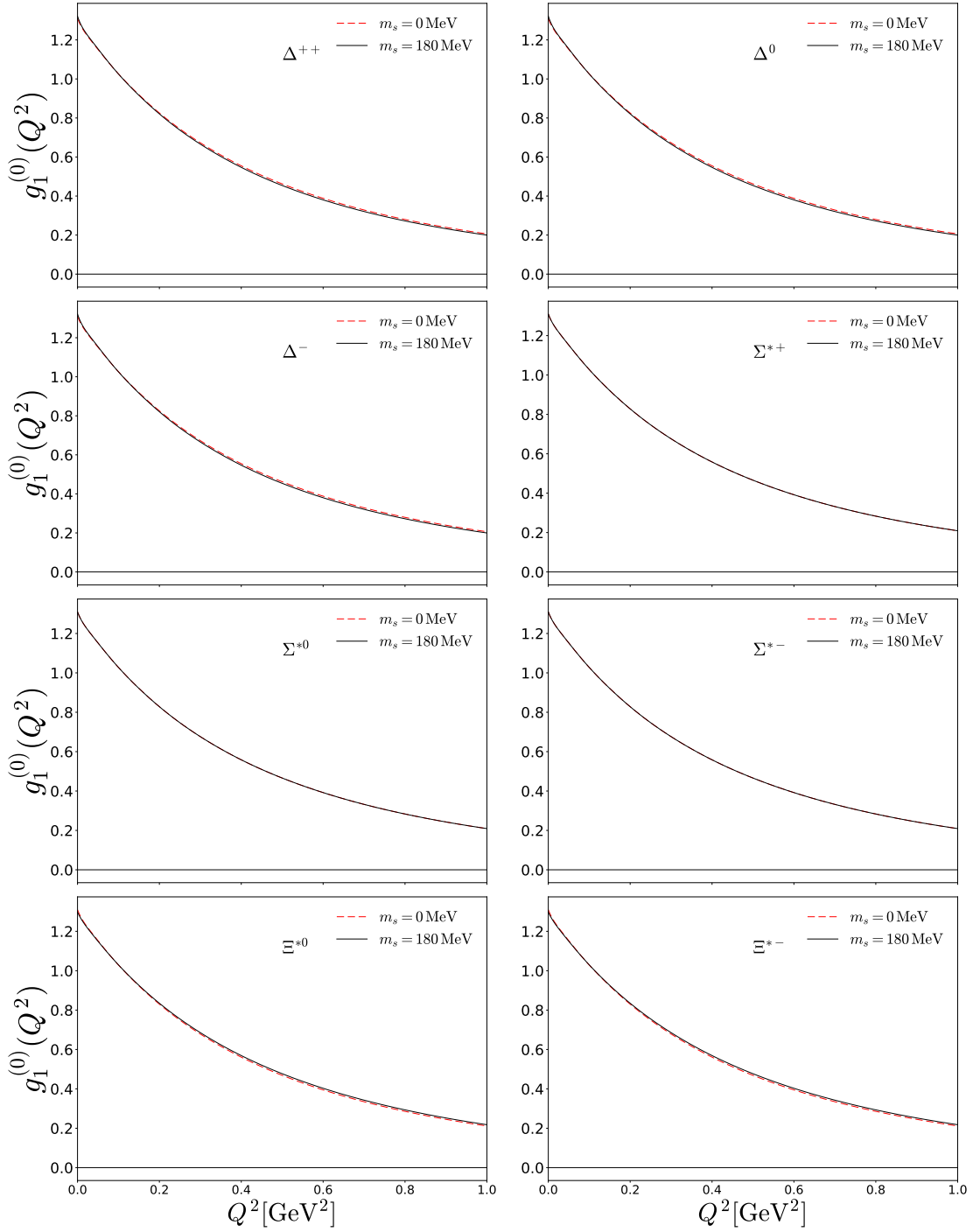


FIG. 7. Effects of the explicit flavor SU(3) symmetry breaking on  $g_1^{(0)B}(Q^2)$  of the baryon decuplet except for the  $\Delta^+$  and  $\Omega^-$  baryons. Notations are the same as in Fig. 1.

component. It is of great interest to compare the axial radius of the  $\Delta^+$  with that of the proton, since the axial radius of the proton is experimentally known. In a recent review [42], the average value of the proton axial radius is given as  $\langle r_A^2 \rangle_p = 0.46(22) \text{ fm}^2$ . Interestingly, the result obtained in the present work for the  $\Delta^+$  axial radius is  $0.447 \text{ fm}^2$ , which is very similar to that of the proton. We want to mention that  $\langle r_A^2 \rangle_p = 0.536 \text{ fm}^2$  was obtained within the same framework, i.e. the  $\chi$ QSM [19]. This indicates that the present results for the triplet axial-vector form factor of  $\Delta^+$  fall off more slowly than the proton one.



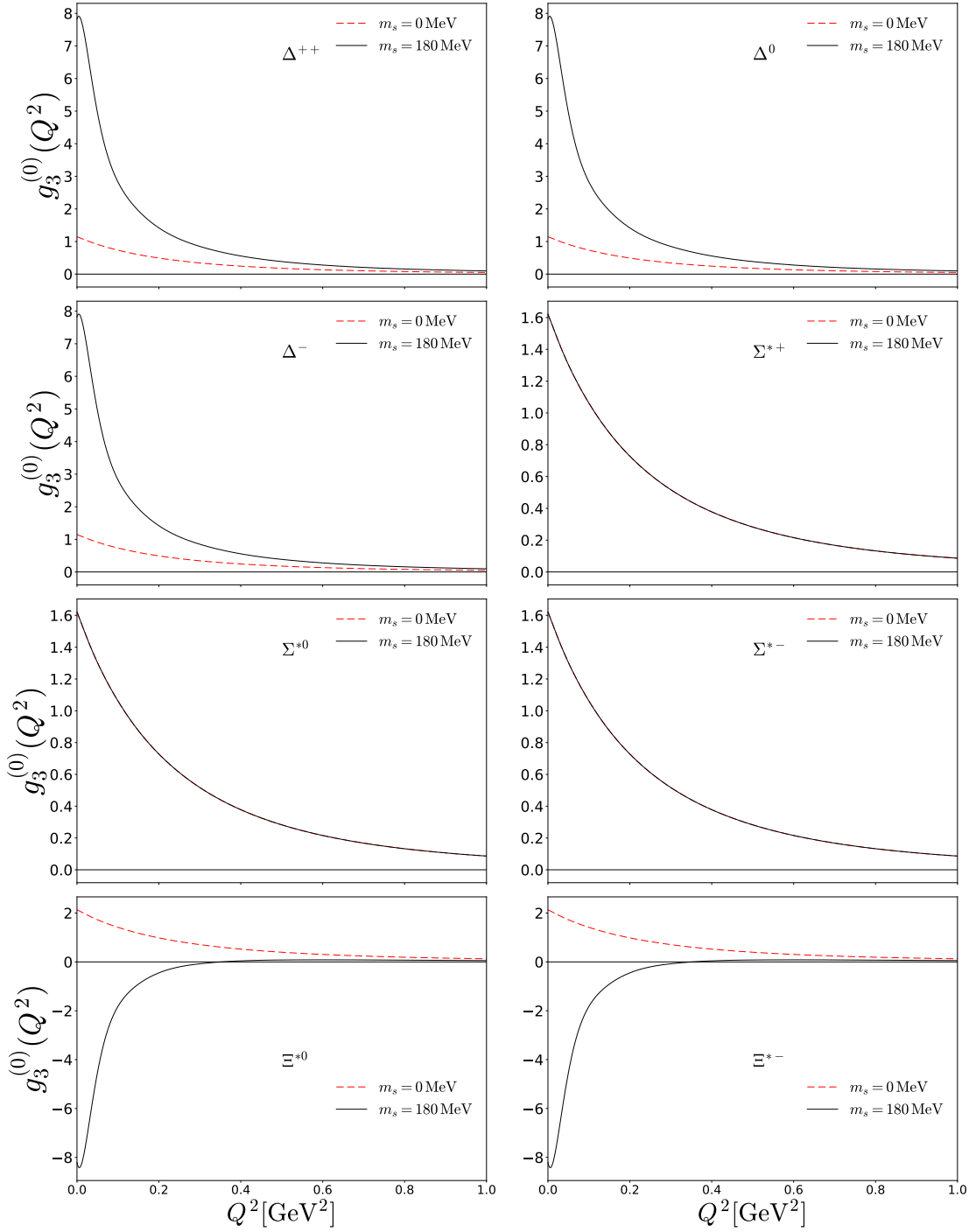


FIG. 8. Effects of the explicit flavor SU(3) symmetry breaking on  $g_3^{(0)B}(Q^2)$  of the baryon decuplet except for the  $\Delta^+$  and  $\Omega^-$  baryons. Notations are the same as in Fig. 1.

A baryon form factor is often parametrized in terms of a dipole-type parametrization given by

$$g_1^{(3)B}(Q^2) = \frac{g_1^{(3)B}(0)}{\left(1 + \frac{Q^2}{M_A^2}\right)^2}, \quad (45)$$

where  $M_A$  is known as the axial mass. This parametrization relates the axial mass to the axial radius by the following

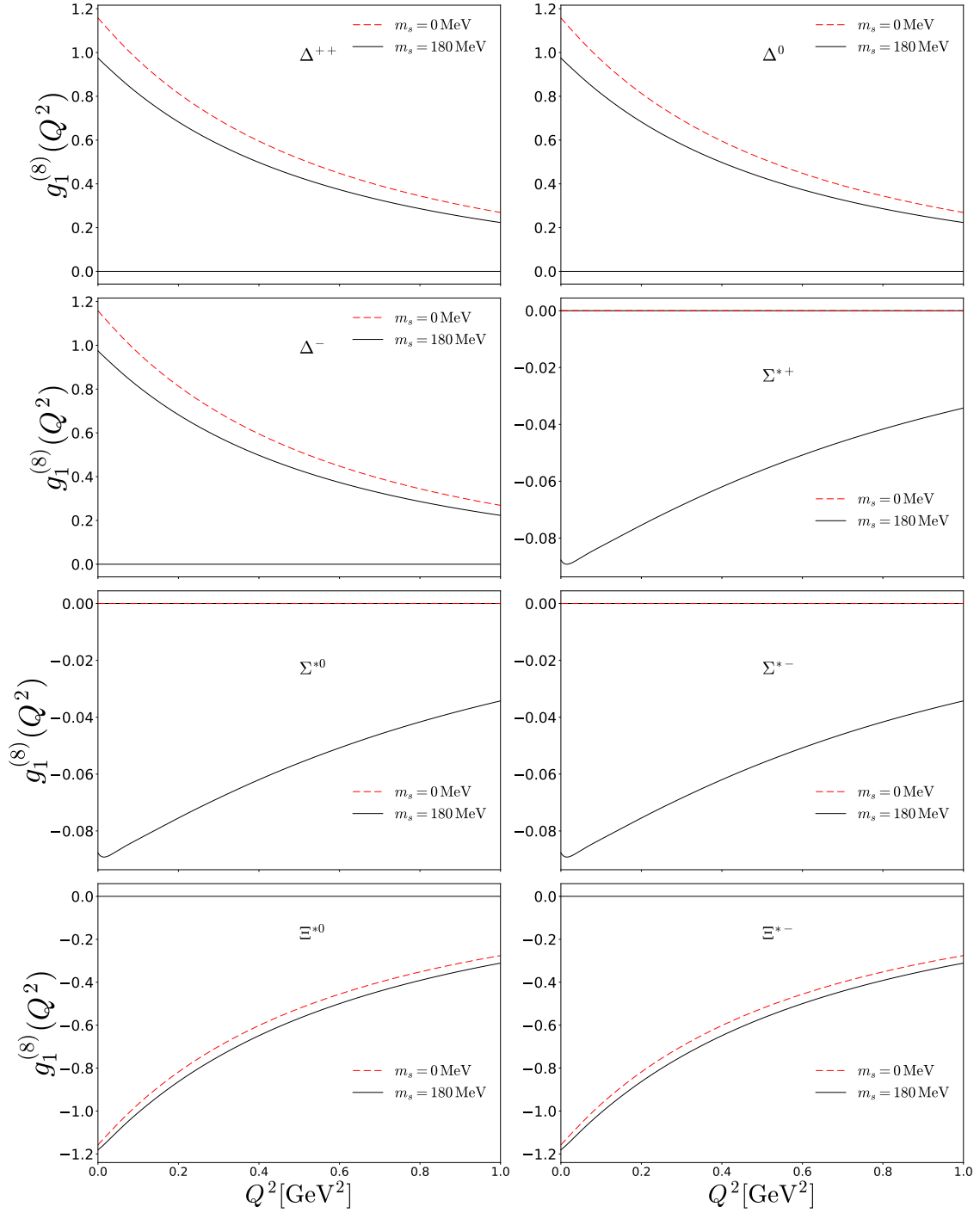


FIG. 9. Effects of the explicit flavor SU(3) symmetry breaking on  $g_1^{(8)B}(Q^2)$  of the baryon decuplet except for the  $\Delta^+$  and  $\Omega^-$  baryons. Notations are the same as in Fig. 1.

relation

$$\langle r_A^2 \rangle = \frac{12}{M_A^2}. \quad (46)$$

The value of  $M_A$  for the proton is also known experimentally [43] whereas those of the baryon decuplet are unknown. Equation (46) already implies that the present result for the  $\Delta^+$  axial mass should be larger than the proton one that was obtained also in Ref. [19],  $M_A(p) = 0.934$  GeV. Indeed, the present result  $M_A(\Delta^+) = 1.023$  GeV is larger than

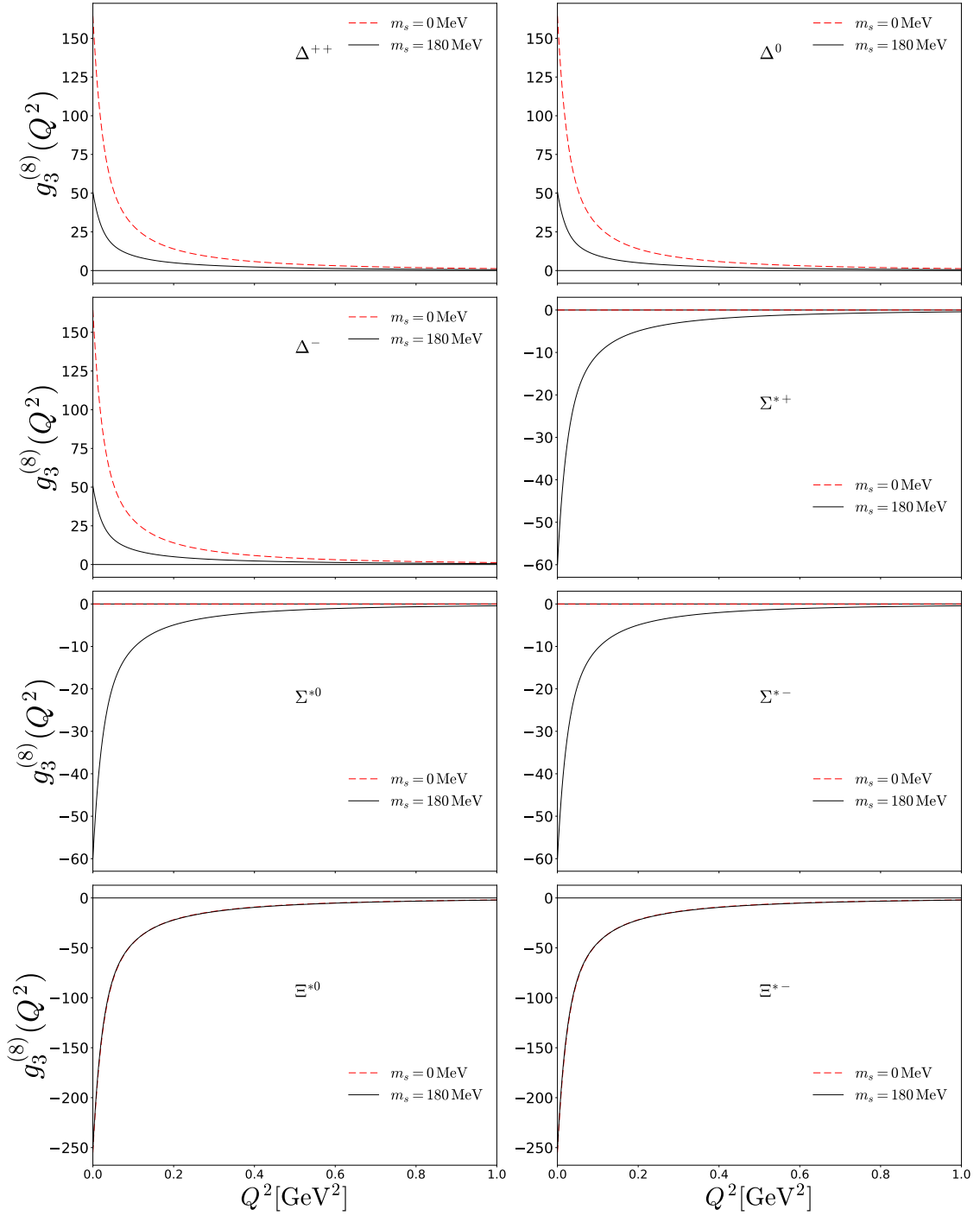


FIG. 10. Effects of the explicit flavor SU(3) symmetry breaking on  $g_3^{(8)B}(Q^2)$  of the baryon decuplet except for the  $\Delta^+$  and  $\Omega^-$  baryons. Notations are the same as in Fig. 1.

that.

Finally, we want to consider another type of the parametrization for the axial-vector form factors. In lattice calculations, a  $p$ -pole parametrization is often adopted [44–46], which can be expressed as

$$g_i^{(3)B}(Q^2) = \frac{g_i^{(3)B}(0)}{\left(1 + \frac{Q^2}{p_i \Lambda_{p_i}^2}\right)^{p_i}}. \quad (47)$$

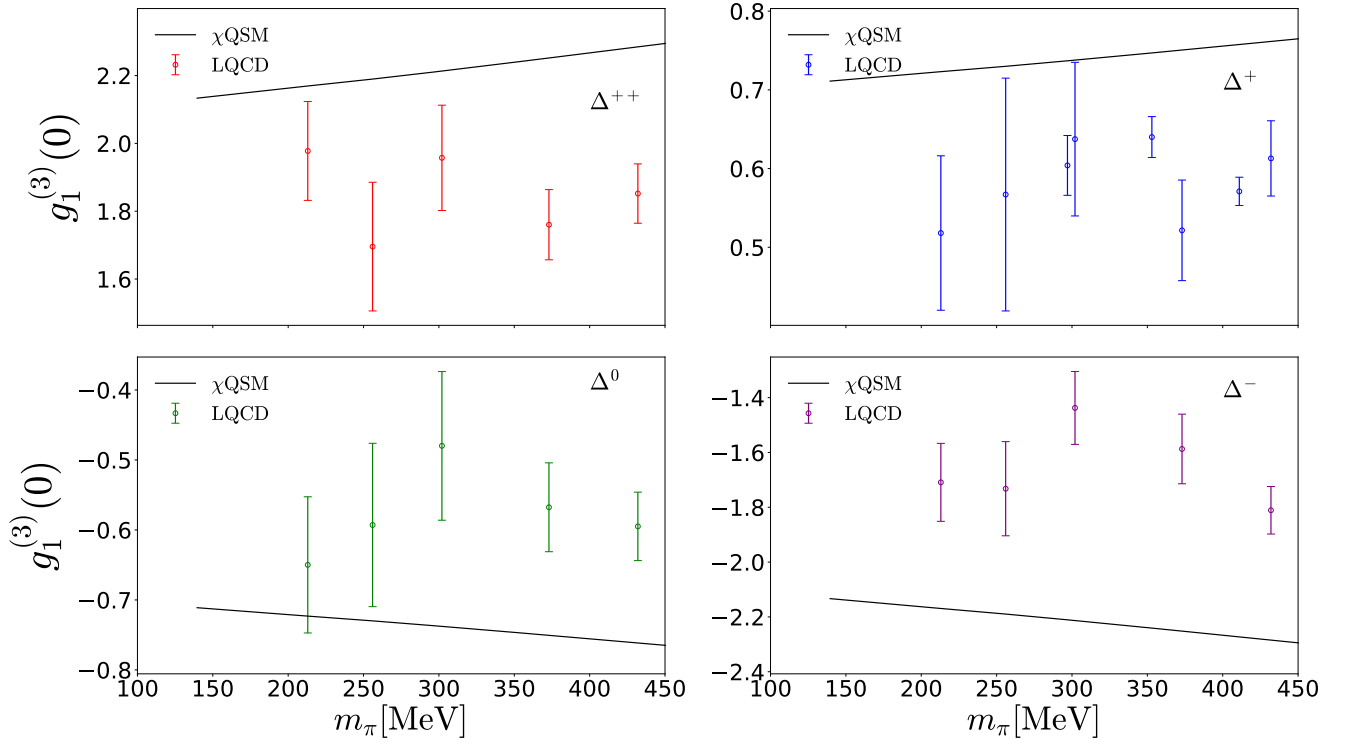


FIG. 11. Dependence of the triplet axial-vector constants of the  $\Delta$  isobars on the pion mass. The numerical results are drawn in the solid curves, which are compared with those from lattice QCD (LQCD) [3, 4].

As drawn in the right panel of Fig. 1, it is rather difficult to fit  $g_3^{(3)\Delta^+}(Q^2)$  by using the dipole-type parametrization. On the other hand, if one parametrizes  $g_3^{(3)\Delta^+}(Q^2)$  by the  $p$ -pole type (47), then we are able to parametrize  $g_3^{(3)\Delta^+}(Q^2)$  by fixing the values of  $p_3 = 1.472$  and  $\Lambda_{p_3} = 0.174$  GeV. Similarly,  $g_3^{(8)}(Q^2)$  can be fitted by using the  $p$ -pole parametrization.

## V. SUMMARY AND CONCLUSION

We aimed at investigating the axial-vector form factors of the baryon decuplet within the framework of the self-consistent chiral quark-soliton model. We consider the rotational  $1/N_c$  corrections and the linear  $m_s$  corrections. Since all the parameters in the model were fixed by reproducing the proton properties, we did not have any parameter to fit. We first computed the triplet axial-vector form factors of the  $\Delta^+$ , because lattice QCD and all other models concentrated on them. We found that the effects of flavor SU(3) symmetry breaking turn out very small on the triplet form factors of  $\Delta^+$ . We then proceeded to compute the singlet axial-vector form factors  $g_{1,3}^{(0)}(Q^2)$ . In this case, there is no leading-order contribution, so that the rotational  $1/N_c$  and linear  $m_s$  corrections are only involved. Concerning the  $g_1^{(0)B}(Q^2)$  form factors, the linear  $m_s$  corrections are almost negligible. On the other hand,  $g_3^{(0)}(Q^2)$  form factors acquire in general large contributions from the  $m_s$  corrections. We then derived the octet axial-vector form factors of the baryon decuplet. The effects of flavor SU(3) symmetry breaking on  $g_1^{(8)}(Q^2)$  are in general very small. However, these linear  $m_s$  corrections come into play as leading-order contributions in the case of the  $\Sigma^*$  octet axial-vector form factors, since the symmetric parts vanish because of the values of their hypercharges. The octet form factors  $g_3^{(8)}(Q^2)$  of the  $\Delta$  isobars get large  $m_s$  contributions whereas those of  $\Xi^*$  and  $\Omega^-$  receive tiny  $m_s$  corrections. We have carefully inspected the dependence of the axial-vector constants as functions of the pion mass to compare the present results with those from lattice QCD. We found that the results of the axial-vector constants turn out larger than the physical ones, when the unphysical values of the pion mass are employed. The magnitudes of the triplet axial-vector constants are in general larger than the lattice data. When it comes to the singlet axial-vector constants, the present results are in very good agreement with the lattice data with  $m_\pi = 432$  MeV used. On the other hand, the results for the octet axial-vector constants are in better agreement with the lattice ones at  $m_\pi = 213$  MeV.

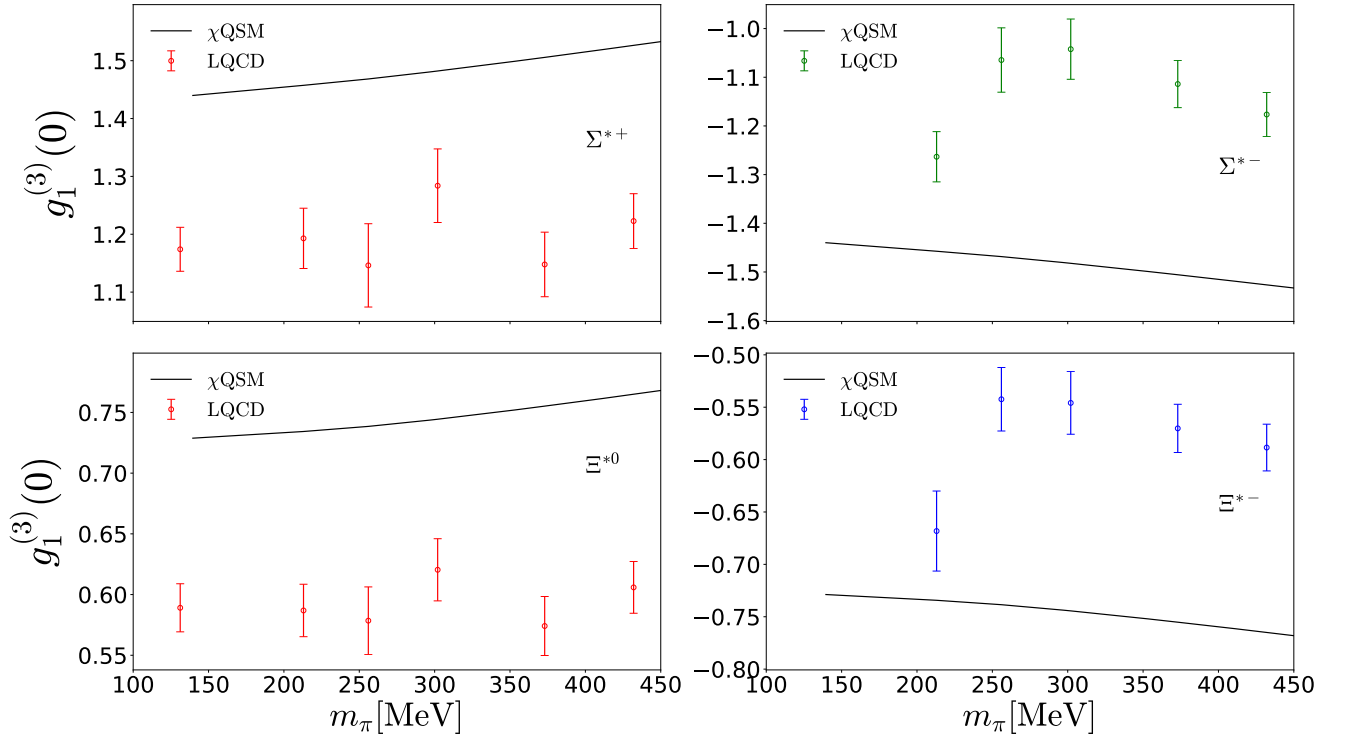


FIG. 12. Dependence of the triplet axial-vector constants of the  $\Sigma^*$  and  $\Xi^*$  on the pion mass. The numerical results are drawn in the solid curves, which are compared with those from lattice QCD (LQCD) [4].

We also presented the results for the axial radii and axial masses of the baryon decuplet. We found that the axial radius of  $\Delta^+$  is very close to the experimental data on the proton axial radius. Compared with the value of the proton axial radius derived from the same model, we observed that the  $\Delta^+$  axial radius is smaller than that of the proton. It indicates that the triplet axial-vector form factor of  $\Delta^+$  falls off more slowly than the proton one. When the strangeness content of a decuplet baryon becomes larger, the corresponding axial radius gets smaller. It indicates that the mass of a baryon may be connected to the axial radius. We also obtained the axial masses, which can be regarded as the inverse of the axial radii. Since the  $p$ -pole parametrization of hadronic form factors is often employed in lattice calculations, we parametrized the present results of the axial-vector form factors, in particular, of the triplet ones, and determined the  $p$  and cutoff mass  $\Lambda_p$ , hoping that results from lattice QCD will appear in the near future.

Since we have computed all possible axial-vector form factors with three different flavors, we are able to express the axial-vector form factors in terms of the flavor-decomposed form factors. This is also very interesting, because we can scrutinize the strange-quark spin content of the  $\Delta$  isobars and the up- and down-quark spin content of the  $\Omega^-$  hyperon. The corresponding work will appear elsewhere. In addition, we can also investigate the transition axial-vector form factors of the baryon decuplet, which will provide further understanding of the structure of the baryon decuplet. The relevant investigation is under way.

## ACKNOWLEDGMENTS

The authors are very grateful to J.-Y. Kim and Gh.-S. Yang for valuable discussions and comments. The present work was supported by Basic Science Research Program through the National Research Foundation of Korea funded by the Ministry of Education, Science and Technology (2018R1A2B2001752 and 2018R1A5A1025563).

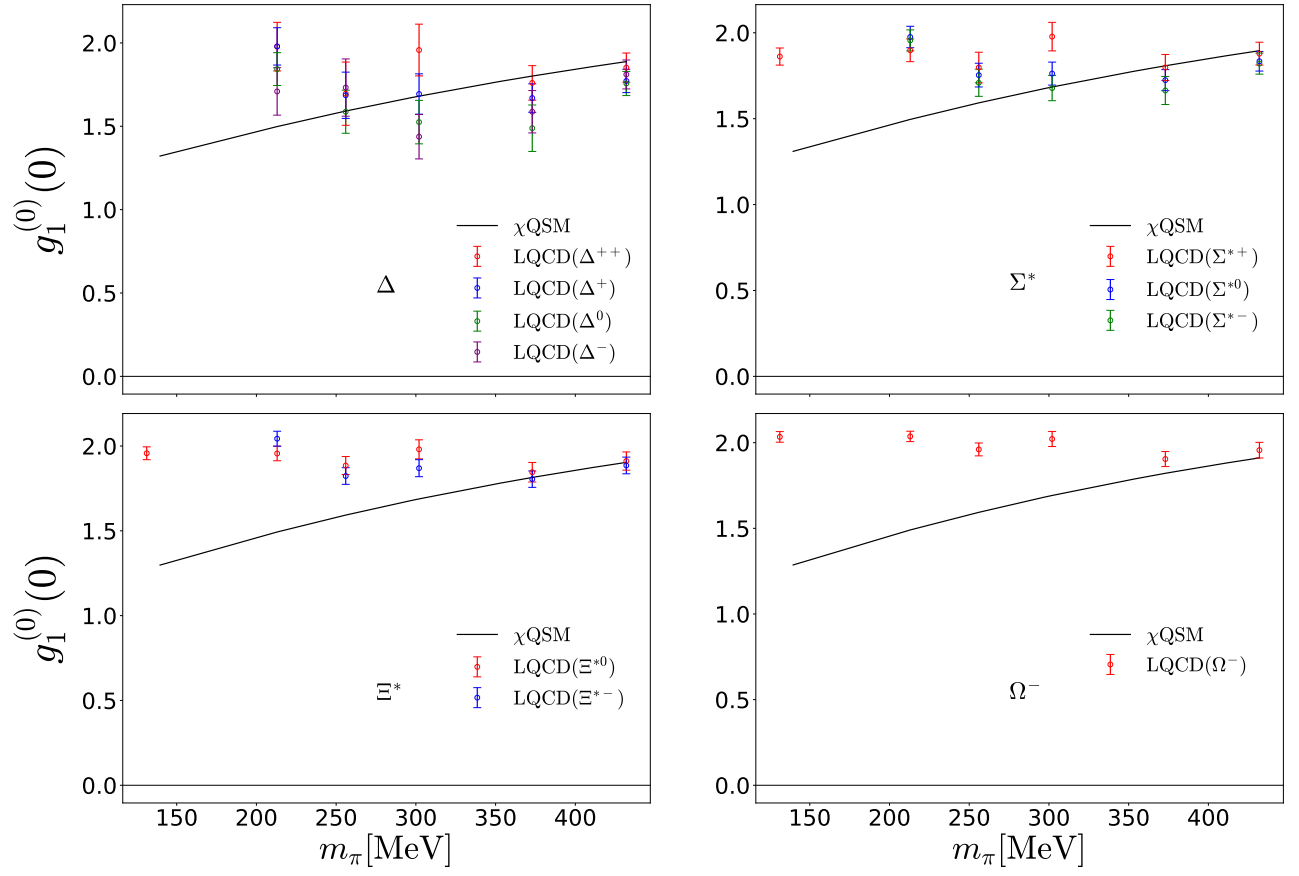


FIG. 13. Dependence of the singlet axial-vector constants  $g_1^{(0)B}(0)$  on the pion mass. The numerical results are drawn in the solid curves, which are compared with those from lattice QCD (LQCD) [4].

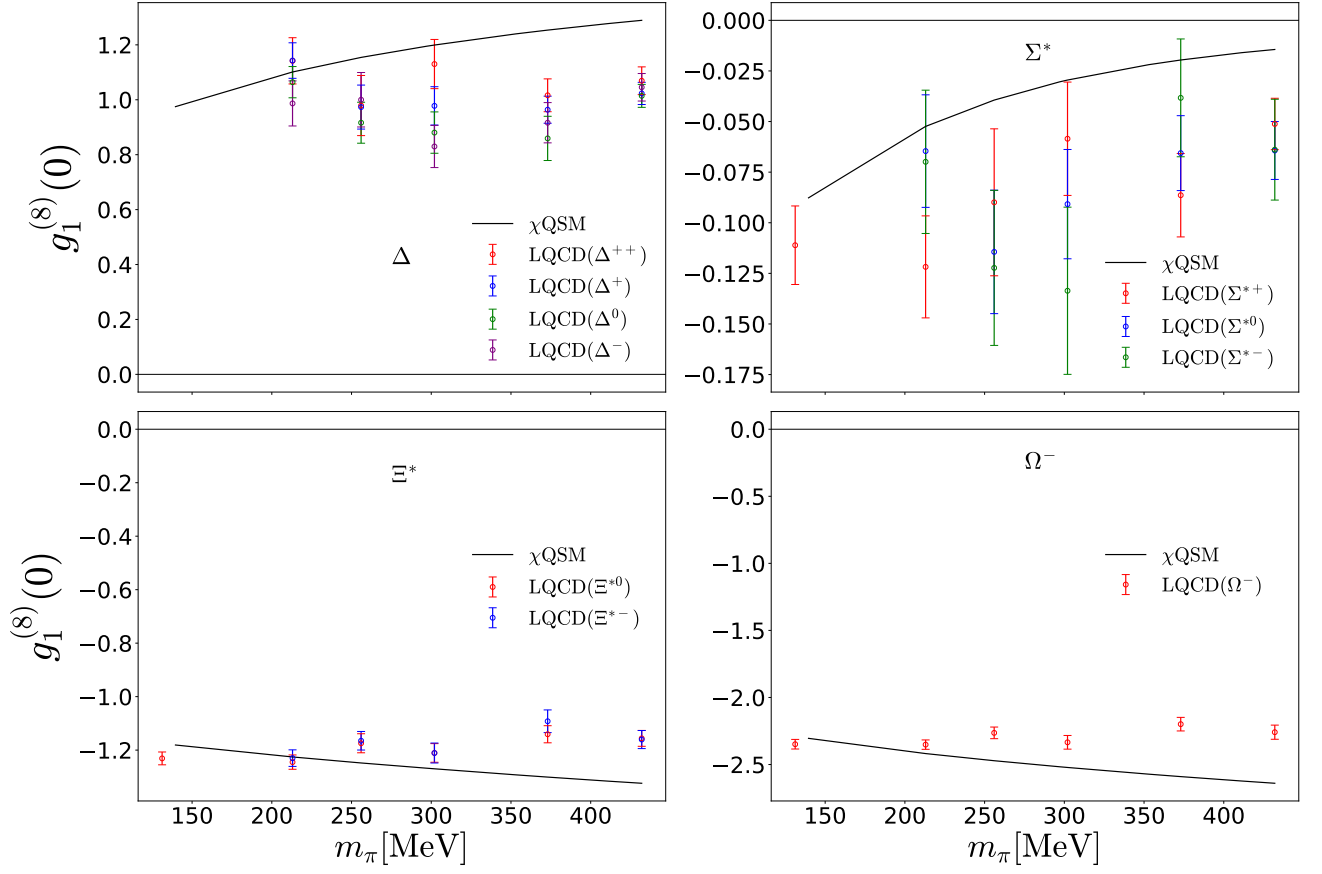


FIG. 14. Dependence of the octet axial-vector constant  $g_1^{(8)B}(0)$  on the pion mass. The numerical results are drawn in the solid curves, which are compared with those from lattice QCD (LQCD) [4]. Note that the expressions for the octet axial-vector constants in Ref. [4] are different from the present one by  $\sqrt{3}$ , so we have considered it for comparison.

TABLE I. Numerical results for the triplet axial-vector constant  $g_1^{(3)B}(0)$  or the axial charge in comparison with those from lattice QCD (LQCD) [3, 4], the relativistic constituent quark model (RCQM) [7, 8], the Light-cone QCD sum rules (LCSR) [9], chiral perturbation theory ( $\chi$ PT) [6] and the perturbative chiral quark model (PCQM) [10].

$g_1^{(3)B}(0)$	$\Delta^{++}$	$\Delta^+$	$\Delta^0$	$\Delta^-$	$\Sigma^{*+}$	$\Sigma^{*0}$	$\Sigma^{*-}$	$\Xi^{*0}$	$\Xi^{*-}$	$\Omega^-$
$m_s = 0 \text{ MeV}$	2.0064	0.6688	-0.6688	-2.0064	1.338	0	-1.338	0.669	-0.669	0
$m_s = 180 \text{ MeV}$	2.1333	0.7111	-0.7111	-2.1333	1.440	0	-1.440	0.729	-0.729	0
LQCD [4] ( $m_\pi = 131.2(13) \text{ MeV}$ )	—	—	—	—	1.1740(380)	—	—	0.5891(198)	—	—
LQCD [4] ( $m_\pi = 213 \text{ MeV}$ )	1.9777(1458)	0.5181(981)	-0.6499(973)	-1.7090(1422)	1.1929(521)	-0.1367(685)	-1.2633(516)	0.5869(216)	-0.6682(382)	—
LQCD [4] ( $m_\pi = 256 \text{ MeV}$ )	1.6956(1897)	0.5670(1479)	-0.5929(1167)	-1.7322(1718)	1.1462(720)	0.0148(542)	-1.0646(661)	0.5785(278)	-0.5424(303)	—
LQCD [3] ( $m_\pi = 297 \text{ MeV}$ )	—	0.604(38)	—	—	—	—	—	—	—	—
LQCD [4] ( $m_\pi = 302 \text{ MeV}$ )	1.9574(1552)	0.6374(976)	-0.4798(1063)	-1.4374(1331)	1.2839(636)	0.0654(444)	-1.0423(619)	0.6204(256)	-0.5459(299)	—
LQCD [3] ( $m_\pi = 353 \text{ MeV}$ )	—	0.640(26)	—	—	—	—	—	—	—	—
LQCD [4] ( $m_\pi = 373 \text{ MeV}$ )	1.7602(1035)	0.5215(639)	-0.5676(635)	-1.5872(1270)	1.1478(558)	-0.0130(323)	-1.1139(485)	0.5741(243)	-0.5702(230)	—
LQCD [3] ( $m_\pi = 411 \text{ MeV}$ )	—	0.571(18)	—	—	—	—	—	—	—	—
LQCD [4] ( $m_\pi = 432 \text{ MeV}$ )	1.8520(875)	0.6129(478)	-0.5949(489)	-1.8108(868)	1.2228(473)	0.0124(244)	-1.1765(450)	0.6059(213)	-0.5885(223)	—
LQCD [3] ( $m_\pi = 490 \text{ MeV}$ )	—	0.578(13)	—	—	—	—	—	—	—	—
LQCD [3] ( $m_\pi = 563 \text{ MeV}$ )	—	0.5887(98)	—	—	—	—	—	—	—	—
$\chi$ PT [6]	2.25*	—	—	—	—	—	—	—	—	—
RCQM[GGE] [7, 8]	2.24*	—	—	—	1.499†	—	—	0.75†	—	—
LCSR [9]	$2.70 \pm 0.6^*$	—	—	—	—	—	—	—	—	—
PCQM [10]	1.863*	—	—	—	1.242†	—	—	0.621†	—	—

\* Since the expressions for the axial-vector constants in Refs. [6–8] and Refs. [9, 10] are different from the present one by  $-2$  and  $-1$  respectively, we have considered these factors for comparison.

† Since the expressions for the axial-vector constants of  $\Sigma^*$  and  $\Xi^*$  in Refs. [7, 10] are different from the present definition by  $-1/\sqrt{2}$  and  $-1$  respectively, we have considered these factors for comparison.



TABLE II. Numerical results for the flavor axial-vector constants except for the axial-vector constants  $g_1^{(a)}(0)$ , axial masses and axial radii. All the results are obtained with flavor SU(3) symmetry breaking taken into account.

$m_s = 180 \text{ MeV}$	$\Delta^{++}$	$\Delta^+$	$\Delta^0$	$\Delta^-$	$\Sigma^{*+}$	$\Sigma^{*0}$	$\Sigma^{*-}$	$\Xi^{*0}$	$\Xi^{*-}$	$\Omega^-$
$g_3^{(3)B}(0)$	346.1	115.4	-115.4	-346.1	303.9	0	-303.9	193.7	-193.7	0
$g_3^{(0)B}(0)$	7.822	7.822	7.822	7.822	1.622	1.622	1.622	-8.204	-8.204	-21.936
$g_3^{(8)B}(0)$	50.8	50.8	50.8	50.8	-60.0	-60.0	-60.0	-251.9	-251.9	-542.8
$\langle r_A^2 \rangle_B [\text{fm}^2]$	0.447	0.447	0.447	0.447	0.438	—	0.438	0.431	0.431	—
$M_A [\text{GeV}]$	1.023	1.023	1.023	1.023	1.033	—	1.033	1.041	1.041	—

### Appendix A: Components of the axial-vector form factors

In this Appendix, the  $Q^2$ -dependent functions in Eqs. (23) and (24) will be expressed explicitly.  $\mathcal{A}_0^B(Q^2)$ ,  $\dots$ ,  $\mathcal{J}_0^B(Q^2)$  are defined by

$$\mathcal{A}_0^B(Q^2) = \frac{N_c M_B}{E_B} \int d^3 r j_0(Q|\mathbf{r}|) \left[ \phi_{\text{val}}^\dagger(\mathbf{r}) \boldsymbol{\sigma} \cdot \boldsymbol{\tau} \phi_{\text{val}}(\mathbf{r}) + \sum_n \phi_n^\dagger(\mathbf{r}) \boldsymbol{\sigma} \cdot \boldsymbol{\tau} \phi_n(\mathbf{r}) \mathcal{R}_1(E_n) \right], \quad (\text{A1})$$

$$\begin{aligned} \mathcal{B}_0^B(Q^2) = \frac{N_c M_B}{E_B} \int d^3 r j_0(Q|\mathbf{r}|) & \left[ \sum_{n \neq \text{val}} \frac{1}{E_{\text{val}} - E_n} \phi_{\text{val}}^\dagger(\mathbf{r}) \boldsymbol{\sigma} \phi_n(\mathbf{r}) \cdot \langle n | \boldsymbol{\tau} | \text{val} \rangle \right. \\ & \left. - \frac{1}{2} \sum_{n,m} \phi_n^\dagger(\mathbf{r}) \boldsymbol{\sigma} \phi_m(\mathbf{r}) \cdot \langle m | \boldsymbol{\tau} | n \rangle \mathcal{R}_5(E_n, E_m) \right], \end{aligned} \quad (\text{A2})$$

$$\begin{aligned} \mathcal{C}_0^B(Q^2) = \frac{N_c M_B}{E_B} \int d^3 r j_0(Q|\mathbf{r}|) & \left[ \sum_{n_0 \neq \text{val}} \frac{1}{E_{\text{val}} - E_{n_0}} \phi_{\text{val}}^\dagger(\mathbf{r}) \boldsymbol{\sigma} \cdot \boldsymbol{\tau} \phi_{n_0}(\mathbf{r}) \langle n_0 | \text{val} \rangle \right. \\ & \left. - \sum_{n,m_0} \phi_n^\dagger(\mathbf{r}) \boldsymbol{\sigma} \cdot \boldsymbol{\tau} \phi_{m_0}(\mathbf{r}) \langle m_0 | n \rangle \mathcal{R}_5(E_n, E_{m_0}) \right], \end{aligned} \quad (\text{A3})$$

$$\begin{aligned} \mathcal{D}_0^B(Q^2) = \frac{N_c M_B}{E_B} \int d^3 r j_0(Q|\mathbf{r}|) & \left[ \sum_{n \neq \text{val}} \frac{\text{sgn}(E_n)}{E_{\text{val}} - E_n} \phi_{\text{val}}^\dagger(\mathbf{r}) (\boldsymbol{\sigma} \times \boldsymbol{\tau}) \phi_n(\mathbf{r}) \cdot \langle n | \boldsymbol{\tau} | \text{val} \rangle \right. \\ & \left. + \frac{1}{2} \sum_{n,m} \phi_n^\dagger(\mathbf{r}) \boldsymbol{\sigma} \times \boldsymbol{\tau} \phi_m(\mathbf{r}) \cdot \langle m | \boldsymbol{\tau} | n \rangle \mathcal{R}_4(E_n, E_m) \right], \end{aligned} \quad (\text{A4})$$

$$\begin{aligned} \mathcal{H}_0^B(Q^2) = \frac{N_c M_B}{E_B} \int d^3 r j_0(Q|\mathbf{r}|) & \left[ \sum_{n \neq \text{val}} \frac{1}{E_{\text{val}} - E_n} \phi_{\text{val}}^\dagger(\mathbf{r}) \boldsymbol{\sigma} \cdot \boldsymbol{\tau} \langle \mathbf{r} | n \rangle \langle n | \gamma^0 | \text{val} \rangle \right. \\ & \left. + \frac{1}{2} \sum_{n,m} \phi_n^\dagger(\mathbf{r}) \boldsymbol{\sigma} \cdot \boldsymbol{\tau} \phi_m(\mathbf{r}) \langle m | \gamma^0 | n \rangle \mathcal{R}_2(E_n, E_m) \right], \end{aligned} \quad (\text{A5})$$

$$\begin{aligned} \mathcal{I}_0^B(Q^2) = \frac{N_c M_B}{E_B} \int d^3 r j_0(Q|\mathbf{r}|) & \left[ \sum_{n \neq \text{val}} \frac{1}{E_{\text{val}} - E_n} \phi_{\text{val}}^\dagger(\mathbf{r}) \boldsymbol{\sigma} \phi_n(\mathbf{r}) \cdot \langle n | \gamma^0 \boldsymbol{\tau} | \text{val} \rangle \right. \\ & \left. + \frac{1}{2} \sum_{n,m} \phi_n^\dagger(\mathbf{r}) \boldsymbol{\sigma} \phi_m(\mathbf{r}) \cdot \langle m | \gamma^0 \boldsymbol{\tau} | n \rangle \mathcal{R}_2(E_n, E_m) \right], \end{aligned} \quad (\text{A6})$$

$$\begin{aligned} \mathcal{J}_0^B(Q^2) = \frac{N_c M_B}{E_B} \int d^3 r j_0(Q|\mathbf{r}|) & \left[ \sum_{n_0 \neq \text{val}} \frac{N_c}{E_{\text{val}} - E_{n_0}} \phi_{\text{val}}^\dagger(\mathbf{r}) \boldsymbol{\sigma} \cdot \boldsymbol{\tau} \phi_{n_0}(\mathbf{r}) \langle n_0 | \gamma^0 | \text{val} \rangle \right. \\ & \left. + N_c \sum_{n,m_0} \phi_n^\dagger(\mathbf{r}) \boldsymbol{\sigma} \cdot \boldsymbol{\tau} \phi_{m_0}(\mathbf{r}) \langle m_0 | \gamma^0 | n \rangle \mathcal{R}_2(E_n, E_{m_0}) \right]. \end{aligned} \quad (\text{A7})$$

where the regularization functions are defined as

$$\mathcal{R}_1(E_n) = \frac{-E_n}{2\sqrt{\pi}} \int_0^\infty \phi(u) \frac{du}{\sqrt{u}} e^{-uE_n^2}, \quad (\text{A8})$$

$$\mathcal{R}_2(E_n, E_m) = \frac{1}{2\sqrt{\pi}} \int_0^\infty \phi(u) \frac{du}{\sqrt{u}} \frac{E_m e^{-uE_m^2} - E_n e^{-uE_n^2}}{E_n - E_m}, \quad (\text{A9})$$

$$\mathcal{R}_4(E_n, E_m) = \frac{1}{2\pi} \int_0^\infty du \phi(u) \int_0^1 d\alpha e^{-\alpha u E_m^2 - (1-\alpha) u E_n^2} \frac{(1-\alpha)E_n - \alpha E_m}{\sqrt{\alpha(1-\alpha)}}, \quad (\text{A10})$$

$$\mathcal{R}_5(E_n, E_m) = \frac{\text{sgn}(E_n) - \text{sgn}(E_m)}{2(E_n - E_m)}. \quad (\text{A11})$$

Here,  $|\text{val}\rangle$  and  $|n\rangle$  denote the state of the valence and sea quarks with the corresponding eigenenergies  $E_{\text{val}}$  and  $E_n$  of the one-body Dirac Hamiltonian  $h(U)$ , respectively.

$\mathcal{A}_2^B(Q^2), \dots, \mathcal{J}_2^B(Q^2)$  are defined by

$$\begin{aligned} \mathcal{A}_2^B(Q^2) = \frac{N_c M_B}{E_B} \int d^3 r j_2(Q|\mathbf{r}|) & \left[ \phi_{\text{val}}^\dagger(\mathbf{r}) \left\{ \sqrt{2\pi} Y_2 \otimes \sigma_1 \right\}_1 \cdot \boldsymbol{\tau} \phi_{\text{val}}(\mathbf{r}) \right. \\ & \left. + \sum_n \phi_n^\dagger(\mathbf{r}) \left\{ \sqrt{2\pi} Y_2 \otimes \sigma_1 \right\}_1 \cdot \boldsymbol{\tau} \phi_n(\mathbf{r}) \mathcal{R}_1(E_n) \right], \end{aligned} \quad (\text{A12})$$

$$\begin{aligned} \mathcal{B}_2^B(Q^2) = \frac{N_c M_B}{E_B} \int d^3 r j_2(Q|\mathbf{r}|) & \left[ \sum_{n \neq \text{val}} \frac{1}{E_{\text{val}} - E_n} \phi_{\text{val}}^\dagger(\mathbf{r}) \left\{ \sqrt{2\pi} Y_2 \otimes \sigma_1 \right\}_1 \phi_n(\mathbf{r}) \cdot \langle n | \boldsymbol{\tau} | \text{val} \rangle \right. \\ & \left. - \frac{1}{2} \sum_{n,m} \phi_n^\dagger(\mathbf{r}) \left\{ \sqrt{2\pi} Y_2 \otimes \sigma_1 \right\}_1 \phi_m(\mathbf{r}) \cdot \langle m | \boldsymbol{\tau} | n \rangle \mathcal{R}_5(E_n, E_m) \right], \end{aligned} \quad (\text{A13})$$

$$\begin{aligned} \mathcal{C}_2^B(Q^2) = \frac{N_c M_B}{E_B} \int d^3 r j_2(Q|\mathbf{r}|) & \left[ \sum_{n_0 \neq \text{val}} \frac{1}{E_{\text{val}} - E_{n_0}} \phi_{\text{val}}^\dagger(\mathbf{r}) \left\{ \sqrt{2\pi} Y_2 \otimes \sigma_1 \right\}_1 \cdot \boldsymbol{\tau} \phi_{n_0}(\mathbf{r}) \langle n_0 | \text{val} \rangle \right. \\ & \left. - \sum_{n,m_0} \phi_n^\dagger(\mathbf{r}) \left\{ \sqrt{2\pi} Y_2 \otimes \sigma_1 \right\}_1 \cdot \boldsymbol{\tau} \phi_{m_0}(\mathbf{r}) \langle m_0 | n \rangle \mathcal{R}_5(E_n, E_{m_0}) \right], \end{aligned} \quad (\text{A14})$$

$$\begin{aligned} \mathcal{D}_2^B(Q^2) = \frac{N_c M_B}{E_B} \int d^3 r j_2(Q|\mathbf{r}|) & \left[ \sum_{n \neq \text{val}} \frac{\text{sgn}(E_n)}{E_{\text{val}} - E_n} \phi_{\text{val}}^\dagger(\mathbf{r}) \left\{ \sqrt{2\pi} Y_2 \otimes \sigma_1 \right\}_1 \times \boldsymbol{\tau} \phi_n(\mathbf{r}) \cdot \langle n | \boldsymbol{\tau} | \text{val} \rangle \right. \\ & \left. + \frac{1}{2} \sum_{n,m} \phi_n^\dagger(\mathbf{r}) \left\{ \sqrt{2\pi} Y_2 \otimes \sigma_1 \right\}_1 \times \boldsymbol{\tau} \phi_m(\mathbf{r}) \cdot \langle m | \boldsymbol{\tau} | n \rangle \mathcal{R}_4(E_n, E_m) \right], \end{aligned} \quad (\text{A15})$$

$$\begin{aligned} \mathcal{H}_2^B(Q^2) = \frac{N_c M_B}{E_B} \int d^3 r j_2(Q|\mathbf{r}|) & \left[ \sum_{n \neq \text{val}} \frac{1}{E_{\text{val}} - E_n} \phi_{\text{val}}^\dagger(\mathbf{r}) \left\{ \sqrt{2\pi} Y_2 \otimes \sigma_1 \right\}_1 \cdot \boldsymbol{\tau} \langle \mathbf{r} | n \rangle \langle n | \gamma^0 | \text{val} \rangle \right. \\ & \left. + \frac{1}{2} \sum_{n,m} \phi_n^\dagger(\mathbf{r}) \left\{ \sqrt{2\pi} Y_2 \otimes \sigma_1 \right\}_1 \cdot \boldsymbol{\tau} \phi_m(\mathbf{r}) \langle m | \gamma^0 | n \rangle \mathcal{R}_2(E_n, E_m) \right], \end{aligned} \quad (\text{A16})$$

$$\begin{aligned} \mathcal{I}_2^B(Q^2) = \frac{N_c M_B}{E_B} \int d^3 r j_2(Q|\mathbf{r}|) & \left[ \sum_{n \neq \text{val}} \frac{1}{E_{\text{val}} - E_n} \phi_{\text{val}}^\dagger(\mathbf{r}) \left\{ \sqrt{2\pi} Y_2 \otimes \sigma_1 \right\}_1 \phi_n(\mathbf{r}) \cdot \langle n | \gamma^0 \boldsymbol{\tau} | \text{val} \rangle \right. \\ & \left. + \frac{1}{2} \sum_{n,m} \phi_n^\dagger(\mathbf{r}) \left\{ \sqrt{2\pi} Y_2 \otimes \sigma_1 \right\}_1 \phi_m(\mathbf{r}) \cdot \langle m | \gamma^0 \boldsymbol{\tau} | n \rangle \mathcal{R}_2(E_n, E_m) \right], \end{aligned} \quad (\text{A17})$$

$$\begin{aligned} \mathcal{J}_2^B(Q^2) = \frac{N_c M_B}{E_B} \int d^3 r j_2(Q|\mathbf{r}|) & \left[ \sum_{n_0 \neq \text{val}} \frac{N_c}{E_{\text{val}} - E_{n_0}} \phi_{\text{val}}^\dagger(\mathbf{r}) \left\{ \sqrt{2\pi} Y_2 \otimes \sigma_1 \right\}_1 \cdot \boldsymbol{\tau} \phi_{n_0}(\mathbf{r}) \langle n_0 | \gamma^0 | \text{val} \rangle \right. \\ & \left. + N_c \sum_{n,m_0} \phi_n^\dagger(\mathbf{r}) \left\{ \sqrt{2\pi} Y_2 \otimes \sigma_1 \right\}_1 \cdot \boldsymbol{\tau} \phi_{m_0}(\mathbf{r}) \langle m_0 | \gamma^0 | n \rangle \mathcal{R}_2(E_n, E_{m_0}) \right]. \end{aligned} \quad (\text{A18})$$

$\mathcal{A}_0^B(Q^2), \dots, \mathcal{J}_0^B(Q^2)$  are defined by

$$\mathcal{A}_0^B(Q^2) = -\frac{4N_c M_B^2}{Q^2} \frac{E_B - M_B}{E_B} \int d^3 r j_0(Q|\mathbf{r}|) \left[ \phi_{\text{val}}(\mathbf{r}) \boldsymbol{\sigma} \cdot \boldsymbol{\tau} \phi_{\text{val}}(\mathbf{r}) + \sum_n \phi_n^\dagger(\mathbf{r}) \boldsymbol{\sigma} \cdot \boldsymbol{\tau} \phi_n(\mathbf{r}) \mathcal{R}_1(E_n) \right], \quad (\text{A19})$$

$$\mathcal{B}_0'^B(Q^2) = -\frac{4N_c M_B^2}{Q^2} \frac{E_B - M_B}{E_B} \int d^3r j_0(Q|\mathbf{r}|) \left[ \sum_{n \neq \text{val}} \frac{1}{E_{\text{val}} - E_n} \phi_{\text{val}}^\dagger(\mathbf{r}) \boldsymbol{\sigma} \phi_n(\mathbf{r}) \cdot \langle n | \boldsymbol{\tau} | \text{val} \rangle \right. \\ \left. - \frac{1}{2} \sum_{n,m} \phi_n^\dagger(\mathbf{r}) \boldsymbol{\sigma} \phi_m(\mathbf{r}) \cdot \langle m | \boldsymbol{\tau} | n \rangle \mathcal{R}_5(E_n, E_m) \right], \quad (\text{A20})$$

$$\mathcal{C}_0'^B(Q^2) = -\frac{4N_c M_B^2}{Q^2} \frac{E_B - M_B}{E_B} \int d^3r j_0(Q|\mathbf{r}|) \left[ \sum_{n_0 \neq \text{val}} \frac{1}{E_{\text{val}} - E_{n_0}} \phi_{\text{val}}^\dagger(\mathbf{r}) \boldsymbol{\sigma} \cdot \boldsymbol{\tau} \phi_{n_0}(\mathbf{r}) \langle n_0 | \text{val} \rangle \right. \\ \left. - \sum_{n,m_0} \phi_n^\dagger(\mathbf{r}) \boldsymbol{\sigma} \cdot \boldsymbol{\tau} \phi_{m_0}(\mathbf{r}) \langle m_0 | n \rangle \mathcal{R}_5(E_n, E_{m_0}) \right], \quad (\text{A21})$$

$$\mathcal{D}_0'^B(Q^2) = -\frac{4N_c M_B^2}{Q^2} \frac{E_B - M_B}{E_B} \int d^3r j_0(Q|\mathbf{r}|) \left[ \sum_{n \neq \text{val}} \frac{\text{sgn}(E_n)}{E_{\text{val}} - E_n} \phi_{\text{val}}^\dagger(\mathbf{r}) (\boldsymbol{\sigma} \times \boldsymbol{\tau}) \phi_n(\mathbf{r}) \cdot \langle n | \boldsymbol{\tau} | \text{val} \rangle \right. \\ \left. + \frac{1}{2} \sum_{n,m} \phi_n^\dagger(\mathbf{r}) \boldsymbol{\sigma} \times \boldsymbol{\tau} \phi_m(\mathbf{r}) \cdot \langle m | \boldsymbol{\tau} | n \rangle \mathcal{R}_4(E_n, E_m) \right], \quad (\text{A22})$$

$$\mathcal{H}_0'^B(Q^2) = -\frac{4N_c M_B^2}{Q^2} \frac{E_B - M_B}{E_B} \int d^3r j_0(Q|\mathbf{r}|) \left[ \sum_{n \neq \text{val}} \frac{1}{E_{\text{val}} - E_n} \phi_{\text{val}}^\dagger(\mathbf{r}) \boldsymbol{\sigma} \cdot \boldsymbol{\tau} \langle n | \gamma^0 | \text{val} \rangle \right. \\ \left. + \frac{1}{2} \sum_{n,m} \phi_n^\dagger(\mathbf{r}) \boldsymbol{\sigma} \cdot \boldsymbol{\tau} \phi_m(\mathbf{r}) \langle m | \gamma^0 | n \rangle \mathcal{R}_2(E_n, E_m) \right], \quad (\text{A23})$$

$$\mathcal{I}_0'^B(Q^2) = -\frac{4N_c M_B^2}{Q^2} \frac{E_B - M_B}{E_B} \int d^3r j_0(Q|\mathbf{r}|) \left[ \sum_{n \neq \text{val}} \frac{1}{E_{\text{val}} - E_n} \phi_{\text{val}}^\dagger(\mathbf{r}) \boldsymbol{\sigma} \phi_n(\mathbf{r}) \cdot \langle n | \gamma^0 \boldsymbol{\tau} | \text{val} \rangle \right. \\ \left. + \frac{1}{2} \sum_{n,m} \phi_n^\dagger(\mathbf{r}) \boldsymbol{\sigma} \phi_m(\mathbf{r}) \cdot \langle m | \gamma^0 \boldsymbol{\tau} | n \rangle \mathcal{R}_2(E_n, E_m) \right], \quad (\text{A24})$$

$$\mathcal{J}_0'^B(Q^2) = -\frac{4N_c M_B^2}{Q^2} \frac{E_B - M_B}{E_B} \int d^3r j_0(Q|\mathbf{r}|) \left[ \sum_{n_0 \neq \text{val}} \frac{N_c}{E_{\text{val}} - E_{n_0}} \phi_{\text{val}}^\dagger(\mathbf{r}) \boldsymbol{\sigma} \cdot \boldsymbol{\tau} \phi_{n_0}(\mathbf{r}) \langle n_0 | \gamma^0 | \text{val} \rangle \right. \\ \left. + N_c \sum_{n,m_0} \phi_n^\dagger(\mathbf{r}) \boldsymbol{\sigma} \cdot \boldsymbol{\tau} \phi_{m_0}(\mathbf{r}) \langle m_0 | \gamma^0 | n \rangle \mathcal{R}_2(E_n, E_{m_0}) \right] \quad (\text{A25})$$

and  $\mathcal{A}_2'^B(Q^2), \dots, \mathcal{J}_2'^B(Q^2)$  are defined by

$$\mathcal{A}_2'^B(Q^2) = -\frac{4N_c M_B^2}{Q^2} \frac{2E_B + M_B}{E_B} \int d^3r j_2(Q|\mathbf{r}|) \left[ \phi_{\text{val}}^\dagger(\mathbf{r}) \left\{ \sqrt{2\pi} Y_2 \otimes \sigma_1 \right\}_1 \cdot \boldsymbol{\tau} \phi_{\text{val}}(\mathbf{r}) \right. \\ \left. + \sum_n \phi_n^\dagger(\mathbf{r}) \left\{ \sqrt{2\pi} Y_2 \otimes \sigma_1 \right\}_1 \cdot \boldsymbol{\tau} \phi_n(\mathbf{r}) \mathcal{R}_1(E_n) \right], \quad (\text{A26})$$

$$\mathcal{B}_2'^B(Q^2) = -\frac{4N_c M_B^2}{Q^2} \frac{2E_B + M_B}{E_B} \int d^3r j_2(Q|\mathbf{r}|) \\ \times \left[ \sum_{n \neq \text{val}} \frac{1}{E_{\text{val}} - E_n} \phi_{\text{val}}^\dagger(\mathbf{r}) \left\{ \sqrt{2\pi} Y_2 \otimes \sigma_1 \right\}_1 \phi_n(\mathbf{r}) \cdot \langle n | \boldsymbol{\tau} | \text{val} \rangle \right. \\ \left. - \frac{1}{2} \sum_{n,m} \phi_n^\dagger(\mathbf{r}) \left\{ \sqrt{2\pi} Y_2 \otimes \sigma_1 \right\}_1 \phi_m(\mathbf{r}) \cdot \langle m | \boldsymbol{\tau} | n \rangle \mathcal{R}_5(E_n, E_m) \right], \quad (\text{A27})$$

$$\begin{aligned}
C_2'^B(Q^2) = & -\frac{4N_c M_B^2}{Q^2} \frac{2E_B + M_B}{E_B} \int d^3r j_2(Q|\mathbf{r}|) \\
& \times \left[ \sum_{n_0 \neq \text{val}} \frac{1}{E_{\text{val}} - E_{n_0}} \phi_{\text{val}}^\dagger(\mathbf{r}) \left\{ \sqrt{2\pi} Y_2 \otimes \sigma_1 \right\}_1 \cdot \boldsymbol{\tau} \phi_{n_0}(\mathbf{r}) \langle n_0 | \text{val} \rangle \right. \\
& \left. - \sum_{n, m_0} \phi_n^\dagger(\mathbf{r}) \left\{ \sqrt{2\pi} Y_2 \otimes \sigma_1 \right\}_1 \cdot \boldsymbol{\tau} \phi_{m_0}(\mathbf{r}) \langle m_0 | n \rangle \mathcal{R}_5(E_n, E_{m_0}) \right], \quad (\text{A28})
\end{aligned}$$

$$\begin{aligned}
\mathcal{D}_2'^B(Q^2) = & -\frac{4N_c M_B^2}{Q^2} \frac{2E_B + M_B}{E_B} \int d^3r j_2(Q|\mathbf{r}|) \\
& \times \left[ \sum_{n \neq \text{val}} \frac{\text{sgn}(E_n)}{E_{\text{val}} - E_n} \phi_{\text{val}}^\dagger(\mathbf{r}) \left\{ \sqrt{2\pi} Y_2 \otimes \sigma_1 \right\}_1 \times \boldsymbol{\tau} \phi_n(\mathbf{r}) \cdot \langle n | \boldsymbol{\tau} | \text{val} \rangle \right. \\
& \left. + \frac{1}{2} \sum_{n, m} \phi_n^\dagger(\mathbf{r}) \left\{ \sqrt{2\pi} Y_2 \otimes \sigma_1 \right\}_1 \times \boldsymbol{\tau} \phi_m(\mathbf{r}) \cdot \langle m | \boldsymbol{\tau} | n \rangle \mathcal{R}_4(E_n, E_m) \right], \quad (\text{A29})
\end{aligned}$$

$$\begin{aligned}
\mathcal{H}_2'^B(Q^2) = & -\frac{4N_c M_B^2}{Q^2} \frac{2E_B + M_B}{E_B} \int d^3r j_2(Q|\mathbf{r}|) \\
& \times \left[ \sum_{n \neq \text{val}} \frac{1}{E_{\text{val}} - E_n} \phi_{\text{val}}^\dagger(\mathbf{r}) \left\{ \sqrt{2\pi} Y_2 \otimes \sigma_1 \right\}_1 \cdot \boldsymbol{\tau} \langle \mathbf{r} | n \rangle \langle n | \gamma^0 | \text{val} \rangle \right. \\
& \left. + \frac{1}{2} \sum_{n, m} \phi_n^\dagger(\mathbf{r}) \left\{ \sqrt{2\pi} Y_2 \otimes \sigma_1 \right\}_1 \cdot \boldsymbol{\tau} \phi_m(\mathbf{r}) \langle m | \gamma^0 | n \rangle \mathcal{R}_2(E_n, E_m) \right], \quad (\text{A30})
\end{aligned}$$

$$\begin{aligned}
\mathcal{I}_2'^B(Q^2) = & -\frac{4N_c M_B^2}{Q^2} \frac{2E_B + M_B}{E_B} \int d^3r j_2(Q|\mathbf{r}|) \\
& \times \left[ \sum_{n \neq \text{val}} \frac{1}{E_{\text{val}} - E_n} \phi_{\text{val}}^\dagger(\mathbf{r}) \left\{ \sqrt{2\pi} Y_2 \otimes \sigma_1 \right\}_1 \phi_n(\mathbf{r}) \cdot \langle n | \gamma^0 \boldsymbol{\tau} | \text{val} \rangle \right. \\
& \left. + \frac{1}{2} \sum_{n, m} \phi_n^\dagger(\mathbf{r}) \left\{ \sqrt{2\pi} Y_2 \otimes \sigma_1 \right\}_1 \phi_m(\mathbf{r}) \cdot \langle m | \gamma^0 \boldsymbol{\tau} | n \rangle \mathcal{R}_2(E_n, E_m) \right], \quad (\text{A31})
\end{aligned}$$

$$\begin{aligned}
\mathcal{J}_2'^B(Q^2) = & -\frac{4N_c M_B^2}{Q^2} \frac{2E_B + M_B}{E_B} \int d^3r j_2(Q|\mathbf{r}|) \\
& \times \left[ \sum_{n_0 \neq \text{val}} \frac{N_c}{E_{\text{val}} - E_{n_0}} \phi_{\text{val}}^\dagger(\mathbf{r}) \left\{ \sqrt{2\pi} Y_2 \otimes \sigma_1 \right\}_1 \cdot \boldsymbol{\tau} \phi_{n_0}(\mathbf{r}) \langle n_0 | \gamma^0 | \text{val} \rangle \right. \\
& \left. + N_c \sum_{n, m_0} \phi_n^\dagger(\mathbf{r}) \left\{ \sqrt{2\pi} Y_2 \otimes \sigma_1 \right\}_1 \cdot \boldsymbol{\tau} \phi_{m_0}(\mathbf{r}) \langle m_0 | \gamma^0 | n \rangle \mathcal{R}_2(E_n, E_{m_0}) \right]. \quad (\text{A32})
\end{aligned}$$

## Appendix B: Matrix elements of the SU(3) Wigner $D$ function

In the following we list the results of the matrix elements of the relevant collective operators for the axial-vector form factors of the baryon decuplet in Table III and IV.

- 
- [1] C. A. Aidala, S. D. Bass, D. Hasch and G. K. Mallot, Rev. Mod. Phys. **85**, 655 (2013).
  - [2] M. L. Goldberger and S. B. Treiman, Phys. Rev. **110**, 1178 (1958).
  - [3] C. Alexandrou, E. B. Gregory, T. Korzec, G. Koutsou, J. W. Negele, T. Sato and A. Tsapalis, Phys. Rev. D **87**, 114513 (2013).

TABLE III. The matrix elements of the single and double Wigner  $D$  function operators.

$J_3 = 3/2$	$\Delta$	$\Sigma^*$	$\Xi^*$	$\Omega$	$J_3 = 3/2$	$\Delta$	$\Sigma^*$	$\Xi^*$	$\Omega$
$\langle B_{\mathcal{R}}   D_{33}^{(8)}   B_{\mathcal{R}} \rangle$	$-\frac{1}{4}T_3$	$-\frac{1}{4}T_3$	$-\frac{1}{4}T_3$	$-\frac{1}{4}T_3$	$\langle B_{\mathcal{R}}   D_{83}^{(8)} D_{38}^{(8)}   B_{\mathcal{R}} \rangle$	$-\frac{5}{84}T_3$	$-\frac{1}{28}T_3$	$-\frac{1}{84}T_3$	0
$\langle B_{\mathcal{R}}   D_{83}^{(8)}   B_{\mathcal{R}} \rangle$	$-\frac{\sqrt{3}}{8}Y$	$-\frac{\sqrt{3}}{8}Y$	$-\frac{\sqrt{3}}{8}Y$	$-\frac{\sqrt{3}}{8}Y$	$\langle B_{\mathcal{R}}   D_{83}^{(8)} D_{88}^{(8)}   B_{\mathcal{R}} \rangle$	$\frac{\sqrt{3}}{56}$	$\frac{\sqrt{3}}{84}$	$-\frac{\sqrt{3}}{56}$	$-\frac{\sqrt{3}}{14}$
$\langle B_{\mathcal{R}}   D_{38}^{(8)} \hat{J}_3   B_{\mathcal{R}} \rangle$	$\frac{\sqrt{3}}{8}T_3$	$\frac{\sqrt{3}}{8}T_3$	$\frac{\sqrt{3}}{8}T_3$	$\frac{\sqrt{3}}{8}T_3$	$\langle B_{\mathcal{R}}   D_{88}^{(8)} D_{33}^{(8)}   B_{\mathcal{R}} \rangle$	$-\frac{5}{84}T_3$	$-\frac{1}{28}T_3$	$-\frac{1}{84}T_3$	0
$\langle B_{\mathcal{R}}   D_{88}^{(8)} \hat{J}_3   B_{\mathcal{R}} \rangle$	$\frac{3}{16}Y$	$\frac{3}{16}Y$	$\frac{3}{16}Y$	$\frac{3}{16}Y$	$\langle B_{\mathcal{R}}   D_{88}^{(8)} D_{83}^{(8)}   B_{\mathcal{R}} \rangle$	$\frac{\sqrt{3}}{56}$	$\frac{\sqrt{3}}{84}$	$-\frac{\sqrt{3}}{56}$	$-\frac{\sqrt{3}}{14}$
$\langle B_{\mathcal{R}}   d_{bc3} D_{3b}^{(8)} \hat{J}_c   B_{\mathcal{R}} \rangle$	$\frac{1}{8}T_3$	$\frac{1}{8}T_3$	$\frac{1}{8}T_3$	$\frac{1}{8}T_3$	$\langle B_{\mathcal{R}}   d_{bc3} D_{8c}^{(8)} D_{3b}^{(8)}   B_{\mathcal{R}} \rangle$	$-\frac{11\sqrt{3}}{252}T_3$	$-\frac{5\sqrt{3}}{84}T_3$	$-\frac{19\sqrt{3}}{252}T_3$	0
$\langle B_{\mathcal{R}}   d_{bc3} D_{8b}^{(8)} \hat{J}_c   B_{\mathcal{R}} \rangle$	$\frac{\sqrt{3}}{16}Y$	$\frac{\sqrt{3}}{16}Y$	$\frac{\sqrt{3}}{16}Y$	$\frac{\sqrt{3}}{16}Y$	$\langle B_{\mathcal{R}}   d_{bc3} D_{8c}^{(8)} D_{8b}^{(8)}   B_{\mathcal{R}} \rangle$	$\frac{5}{56}$	$-\frac{1}{42}$	$-\frac{5}{56}$	$-\frac{3}{28}$

TABLE IV. The transition matrix elements of the single Wigner  $D$  function operators coming from the 27-plet and 35-plet component of the baryon wavefunctions.

$J_3 = 3/2$	$\Delta$	$\Sigma^*$	$\Xi^*$	$\Omega$	$J_3 = 3/2$	$\Delta$	$\Sigma^*$	$\Xi^*$	$\Omega$
$\langle B_{27}   D_{33}^{(8)}   B_{\mathcal{R}} \rangle$	$-\frac{1}{12}\sqrt{\frac{5}{6}}T_3$	$-\frac{1}{8}T_3$	$-\frac{7}{12}\sqrt{\frac{1}{6}}T_3$	0	$\langle B_{35}   D_{33}^{(8)}   B_{\mathcal{R}} \rangle$	$-\frac{1}{20}\sqrt{\frac{1}{14}}T_3$	$-\frac{1}{8}\sqrt{\frac{1}{35}}T_3$	$-\frac{1}{4}\sqrt{\frac{1}{70}}T_3$	0
$\langle B_{27}   D_{83}^{(8)}   B_{\mathcal{R}} \rangle$	$\frac{1}{8}\sqrt{\frac{5}{2}}$	$\frac{1}{4}\sqrt{\frac{1}{3}}$	$\frac{1}{8}\sqrt{\frac{1}{2}}$	0	$\langle B_{35}   D_{83}^{(8)}   B_{\mathcal{R}} \rangle$	$-\frac{1}{8}\sqrt{\frac{3}{14}}$	$-\frac{1}{4}\sqrt{\frac{3}{35}}$	$-\frac{3}{8}\sqrt{\frac{3}{70}}$	$-\frac{1}{4}\sqrt{\frac{3}{35}}$
$\langle B_{27}   D_{38}^{(8)} J_3   B_{\mathcal{R}} \rangle$	$-\frac{1}{8}\sqrt{\frac{5}{2}}T_3$	$-\frac{3\sqrt{3}}{16}T_3$	$-\frac{7}{8}\sqrt{\frac{1}{2}}T_3$	0	$\langle B_{35}   D_{38}^{(8)} J_3   B_{\mathcal{R}} \rangle$	$\frac{1}{8}\sqrt{\frac{3}{14}}T_3$	$\frac{1}{16}\sqrt{\frac{15}{7}}T_3$	$\frac{1}{8}\sqrt{\frac{15}{14}}T_3$	0
$\langle B_{27}   D_{88}^{(8)} J_3   B_{\mathcal{R}} \rangle$	$\frac{3}{16}\sqrt{\frac{15}{2}}$	$\frac{3}{8}$	$\frac{3}{16}\sqrt{\frac{3}{2}}$	0	$\langle B_{35}   D_{88}^{(8)} J_3   B_{\mathcal{R}} \rangle$	$\frac{15}{16}\sqrt{\frac{1}{14}}$	$\frac{3}{8}\sqrt{\frac{5}{7}}$	$\frac{9}{16}\sqrt{\frac{5}{14}}$	$\frac{3}{8}\sqrt{\frac{5}{7}}$
$\langle B_{27}   d_{ab3} D_{3a}^{(8)} J_b   B_{\mathcal{R}} \rangle$	$-\frac{1}{24}\sqrt{\frac{5}{6}}T_3$	$-\frac{1}{16}T_3$	$-\frac{7}{24}\sqrt{\frac{1}{6}}T_3$	0	$\langle B_{35}   d_{ab3} D_{3a}^{(8)} J_b   B_{\mathcal{R}} \rangle$	$-\frac{1}{8}\sqrt{\frac{1}{14}}T_3$	$-\frac{1}{16}\sqrt{\frac{5}{7}}T_3$	$-\frac{1}{8}\sqrt{\frac{5}{14}}T_3$	0
$\langle B_{27}   d_{ab3} D_{8a}^{(8)} J_b   B_{\mathcal{R}} \rangle$	$\frac{1}{16}\sqrt{\frac{5}{2}}$	$\frac{1}{8}\sqrt{\frac{1}{3}}$	$\frac{1}{16}\sqrt{\frac{1}{2}}$	0	$\langle B_{35}   d_{ab3} D_{8a}^{(8)} J_b   B_{\mathcal{R}} \rangle$	$-\frac{5}{16}\sqrt{\frac{3}{14}}$	$-\frac{1}{8}\sqrt{\frac{15}{7}}$	$-\frac{3}{16}\sqrt{\frac{15}{14}}$	$-\frac{1}{8}\sqrt{\frac{15}{7}}$

- [4] C. Alexandrou, K. Hadjiyiannakou and C. Kallidonis, Phys. Rev. D **94**, 034502 (2016).
- [5] E. E. Jenkins and A. V. Manohar, Phys. Lett. B **259**, 353 (1991).
- [6] F. J. Jiang and B. C. Tiburzi, Phys. Rev. D **78**, 017504 (2008).
- [7] K. S. Choi, W. Plessas and R. F. Wagenbrunn, Phys. Rev. D **82**, 014007 (2010).
- [8] K. S. Choi and W. Plessas, Few Body Syst. **54**, 1055 (2013).
- [9] A. Kucukarslan, U. Ozdem and A. Ozpineci, Phys. Rev. D **90**, 054002 (2014).
- [10] X. Y. Liu, D. Samart, K. Khosonthongkee, A. Limphirath, K. Xu and Y. Yan, Phys. Rev. C **97**, 055206 (2018).
- [11] D. Diakonov, V. Y. Petrov and P. V. Pobylitsa, Nucl. Phys. B **306**, 809 (1988).
- [12] D. Diakonov, [hep-ph/9802298].
- [13] A. Blotz, D. Diakonov, K. Goeke, N. W. Park, V. Petrov and P. V. Pobylitsa, Nucl. Phys. A **555**, 765 (1993).
- [14] E. Witten, Nucl. Phys. B **160**, 57 (1979).
- [15] E. Witten, Nucl. Phys. B **223**, 433 (1983).
- [16] H.-Ch. Kim, A. Blotz, M. V. Polyakov and K. Goeke, Phys. Rev. D **53**, 4013 (1996).
- [17] T. Ledwig, A. Silva and M. Vanderhaeghen, Phys. Rev. D **79**, 094025 (2009).
- [18] J. Y. Kim and H.-Ch. Kim, Eur. Phys. J. C **79**, 570 (2019).
- [19] A. Silva, H.-Ch. Kim, D. Urbano and K. Goeke, Phys. Rev. D **72**, 094011 (2005).
- [20] H.-Ch. Kim, A. Blotz, C. Schneider and K. Goeke, Nucl. Phys. A **596**, 415 (1996).
- [21] H.-Ch. Kim, M. V. Polyakov and K. Goeke, Phys. Rev. D **53**, 4715 (1996).
- [22] H.-Ch. Kim, M. V. Polyakov and K. Goeke, Phys. Lett. B **387**, 577 (1996).
- [23] T. Ledwig, A. Silva and H.-Ch. Kim, Phys. Rev. D **82**, 034022 (2010).

- [24] T. Ledwig, A. Silva and H.-Ch. Kim, Phys. Rev. D **82**, 054014 (2010).
- [25] K. Goeke, J. Grabis, J. Ossmann, M. V. Polyakov, P. Schweitzer, A. Silva and D. Urbano, Phys. Rev. D **75**, 094021 (2007).
- [26] J. Y. Kim and H.-Ch. Kim, Phys. Rev. D **97**, 114009 (2018).
- [27] J. Y. Kim and H.-Ch. Kim, arXiv:1912.01437 [hep-ph].
- [28] M. D. Scadron, Phys. Rev. **165**, 1640 (1968).
- [29] W. Rarita and J. Schwinger, Phys. Rev. **60**, 61 (1941).
- [30] H. F. Jones and M. D. Scadron, Annals Phys. **81**, 1 (1973).
- [31] H. J. Weber and H. Arenhovel, Phys. Rept. **36**, 277 (1978).
- [32] M. A. B. Beg and A. Zepeda, Phys. Rev. D **6**, 2912 (1972).
- [33] W. Pauli and S. M. Dancoff, Phys. Rev. **62**, 85 (1942).
- [34] B. L. Ioffe, Nucl. Phys. B **188**, 317 (1981). Erratum: [Nucl. Phys. B **191**, 591 (1981)].
- [35] C. V. Christov, A. Blotz, H. C. Kim, P. Pobylitsa, T. Watabe, T. Meissner, E. Ruiz Arriola and K. Goeke, Prog. Part. Nucl. Phys. **37**, 91 (1996).
- [36] J. Y. Kim, H.-Ch. Kim and G. S. Yang, Phys. Rev. D **98**, 054004 (2018).
- [37] T. Ledwig, H.-Ch. Kim and K. Goeke, Phys. Rev. D **78**, 054005 (2008).
- [38] M. Praszalowicz, T. Watabe and K. Goeke, Nucl. Phys. A **647**, 49 (1999).
- [39] S. J. Brodsky, J. R. Ellis and M. Karliner, Phys. Lett. B **206**, 309 (1988).
- [40] K. Goeke, J. Ossmann, P. Schweitzer and A. Silva, Eur. Phys. J. A **27**, 77 (2006).
- [41] K. Goeke, J. Grabis, J. Ossmann, P. Schweitzer, A. Silva and D. Urbano, Phys. Rev. C **75**, 055207 (2007).
- [42] R. J. Hill, P. Kammel, W. J. Marciano and A. Sirlin, Rept. Prog. Phys. **81**, 096301 (2018).
- [43] A. Liesenfeld *et al.* [A1 Collaboration], Phys. Lett. B **468**, 20 (1999).
- [44] M. Göckeler *et al.* [QCDSF and UKQCD Collaborations], Phys. Rev. Lett. **98**, 222001 (2007).
- [45] D. Brommel *et al.* [QCDSF/UKQCD Collaboration], Eur. Phys. J. C **51**, 335 (2007).
- [46] D. Brommel *et al.* [QCDSF and UKQCD Collaborations], Phys. Rev. Lett. **101**, 122001 (2008).